https://doi.org/10.5194/egusphere-2022-749
Preprint. Discussion started: 8 September 2022

Theoretical assessment of the ability of the MicroCarb satellite city-scan observing mode to estimate urban CO_2 emissions

Kai Wu[1], Paul I. Palmer[1,2], Dien Wu[3], Denis Jouglet[4], Liang Feng[1,2], and Tom Oda[5,6,7]

[1]School of GeoSciences, University of Edinburgh, Edinburgh, UK
[2]National Centre for Earth Observation, University of Edinburgh, Edinburgh, UK
[3]Division of Geological and Planetary Sciences, California Institute of Technology, Pasadena, CA, USA
[4]Centre National d'Etudes Spatiales, Toulouse, France
[5]Earth from Space Institute, Universities Space Research Association, Columbia, MD, USA
[6]Department of Atmospheric and Oceanic Science, University of Maryland, College Park, MD, USA
[7]Graduate School of Engineering, Osaka University, Suita, Osaka, Japan

Correspondence: Kai Wu (kwu2@ed.ac.uk) and Paul I. Palmer (pip@ed.ac.uk)

Abstract.

We assess the theoretical capability of the upcoming French-UK MicroCarb satellite, which has a city-scan observing mode, to determine integrated urban emissions of carbon dioxide (CO_2). To achieve this we report results from a series of closed-loop numerical experiments that use an atmospheric transport model with anthropogenic and biogenic fluxes to determine the corresponding changes in atmospheric CO_2 column, accounting for changes in measurement coverage due to clouds loading. We use a Maximum *A Posteriori* inverse method to infer the CO_2 fluxes based on the measurements and the *a priori* information. Using an urban CO_2 inversion system, we explore the relative performance of alternative two-sweep and three-sweep city observing strategies to quantify CO_2 emissions over the cities of Paris and London in different months when biospheric fluxes vary in magnitude. We find that both the two-sweep and three-sweep observing modes are able to reduce *a priori* flux errors by 20–40% over Paris and London. The three-sweep observing strategy, which generally outperforms the two-sweep mode, can retrieve the total emissions of the truth within 7% over Paris and 21% over London, by virtue of its wider scan area that typically yields more cloud-free scenes. The performance of the limited-domain city-mode observing strategies is sensitive to cloud coverage and particularly sensitive to the prevailing wind direction. We also find that seasonal photosynthetic uptake of CO_2 by the urban biosphere weakens atmospheric CO_2 gradients across both cities thereby reducing the sensitivity of urban CO_2 enhancements and subsequently compromising the ability of MicroCarb to estimate urban CO_2 emissions. This suggests that additional trace gases co-emitted with anthropogenic CO_2 emissions, but unaffected by the land biosphere, are needed to quantify sub-city scale CO_2 emissions during months when the urban biosphere is particularly active.

1 Introduction

Over 70% of global energy-related anthropogenic CO_2 emissions are from urban areas (Bulkeley, 2013). Recent studies have empirically related city-scale CO_2 emission estimates with urban population density (Wu et al., 2020; Yang et al., 2020). With urbanization rates projected to increase to 68% by 2050 (Chaouad and Verzeroli, 2018), urban CO_2 emissions have become

https://doi.org/10.5194/egusphere-2022-749
Preprint. Discussion started: 8 September 2022

a focus of emission mitigation efforts to limit global warming to 1.5°C above pre-industrial levels and to achieve carbon neutrality by 2050 (Masson-Delmotte et al., 2018, 2021). Satellite-based measurements of atmospheric CO_2 are dedicated to support the monitoring of surface CO_2 fluxes (Crisp et al., 2017). Here, we explore the theoretical potential of the city-observing mode of the upcoming French-UK MicroCarb satellite to quantify urban emissions of CO_2.

Quantifying urban-scale greenhouse gas emissions is currently limited to individual and networks of ground-based (*in situ*) instruments (Lopez et al., 2013; Bréon et al., 2015; Turner et al., 2016; Helfter et al., 2016; Lauvaux et al., 2016; Davis et al., 2017; Verhulst et al., 2017; Sargent et al., 2018; Kunik et al., 2019) and to sensors on mobile platforms (Mallia et al., 2020; Ionov et al., 2021; Makarova et al., 2021). Integrated emissions of CO_2 from the largest emission hotspots, including cities, can already be observed along individual orbits using existing low Earth orbiting satellites of GOSAT (Yokota et al., 2009; Morino et al., 2011; Kort et al., 2012; Janardanan et al., 2016) and OCO-2 (Hakkarainen et al., 2016; Schwandner et al., 2017; Crisp et al., 2017; Eldering et al., 2017) either directly as X_{CO_2}, the atmospheric column-averaged dry-air mole fraction of CO_2 (Ye et al., 2020; Zheng et al., 2020; Lei et al., 2021), or via monitoring tropospheric NO_2 (Konovalov et al., 2016; Goldberg et al., 2019; Reuter et al., 2019; Hakkarainen et al., 2021; Park et al., 2021; Finch et al., 2022). The main advantage of using data from low Earth orbiting satellite is their global coverage, subject to cloud cover and atmospheric aerosol loading (O'Dell et al., 2018). The current generation of satellites employ instruments with small ground footprints and relatively long revisit time (three to 16 days), resulting in a low probability of sampling clear skies over individual cities. This capability continues with GOSAT-2 (Suto et al., 2021) and TanSat (Cai et al., 2014; Liu et al., 2018; Yang et al., 2018), and in the near future by the Copernicus CO_2 Monitoring Mission that includes cross-track sampling (Sierk et al., 2021) that will increase the probability of clear-sky data being collected over cities.

The NASA Orbiting Carbon Observatory (OCO-3), installed on the International Space Station in 2019 (Eldering et al., 2019; Taylor et al., 2020) has an external pointing mirror assembly that facilitates Snapshot Area Maps (SAMs) that describe fore- and aft- sampling of a limited area of interest on the ground such as a large city. Early analysis of OCO-3 data over the Los Angeles Basin (Kiel et al., 2021) revealed intra-urban X_{CO_2} gradients, reflecting the mosaic of emission types and magnitudes across the region thereby illustrating the value of these sampling approaches. Using a limited number of SAMs, this study reported elevated X_{CO_2} values have a median value of 2 ppm, ranging from 0 to 6 ppm. A recent study has combined OCO-3 X_{CO_2} data with carbon monoxide (CO) retrievals from the TROPOspheric Monitoring Instrument over Los Angeles and Shanghai, Baotou, and Zibo in China to attribute and contrast intra-city gradients of CO_2 using inferred estimates of combustion efficiency (Wu et al., 2022a).

MicroCarb, due for launch in late 2023/early 2024, will be the first European satellite dedicated to measuring atmospheric CO_2 with sufficient precision to detect the changes associated with surface fluxes across the world (https://microcarb.cnes.fr/en). Data from MicroCarb will ensure continuity of collecting atmospheric CO_2 from low Earth orbit, e.g., GOSAT, OCO-2, TanSat, and GOSAT-2. The instrument is a passive spectrometer that uses an echelle grating to disperse reflected sunlight (Pascal et al., 2017) into four short-wave infrared bands sensitive to changes in atmospheric CO_2 (1.61 μm and 2.06 μm) and O_2 (0.76 μm and 1.27 μm) used as a proxy for the atmospheric path length accounting for changes in, for example, orography, aerosols, and clouds (Bertaux et al., 2020). MicroCarb will employ three observing modes: (1) nadir measurements over land, which have

https://doi.org/10.5194/egusphere-2022-749
Preprint. Discussion started: 8 September 2022

a ground pixel size of 4.5 km (across track) × 8.9 km (along track); (2) sunglint measurements over oceans and lakes with a variable footprint size but with the same order of magnitude as the nadir configuration; and (3) city-mode observations that collect a series of fore- and aft- measurements of atmospheric CO_2 at a spatial resolution of 2.25 km × 2.25 km as the satellite pass over a target region, e.g., a city or a calibration reference point collocated with a ground-based remote sensing instrument (Wunch et al., 2011, 2017).

We use a series of closed-loop numerical experiments (i.e., observing system simulation experiments) to evaluate the theoretical ability of MicroCarb city-mode measurements to estimate integrated city-wide CO_2 emissions over Paris and London, considering a realistic instrument noise model. We report results in three different months, accounting for differences in cloud cover, prevailing wind patterns, and biospheric CO_2 fluxes. We also compare the performance of two proposed sampling strategies being considered by MicroCarb involving two and three measurement sweeps across a city. In the next section, we describe our modelling approach and provide details about how we simulate MicroCarb measurements. In section 3, we report our results, including a sensitivity analyses. We conclude the study in section 4, including a discussion of our results and how we anticipate they will be used when MicroCarb is launched.

2 Data and Methods

Here we describe the MicroCarb instrument and its city-mode sampling strategy, and the individual components of the closed-loop numerical experiments (Figure 1) focused on Paris and London during April, July, and December 2018.

2.1 MicroCarb city-mode configuration

The two-sweep and three-sweep city-scan sampling configurations (Figure 2) are being considered by the MicroCarb science team. Both city-scan configurations cover a city the size of Paris or London. For the nominal nadir acquisition mode, each satellite sounding is acquired by a detector matrix using 90 pixels in a dimension corresponding to the spatial across-track (ACT) swath and 1024 pixels in the other dimension corresponding to the spectrum, which is used for the four infrared bands described above. Each individual sounding results from the binning of 30 pixels ACT. The spatial along-track (ALT) dimension is acquired by the satellite velocity during the 1.3 s integration time, which leads to the nominal pattern of three soundings of 4.5 km ACT x 8.9 km ALT, leading to a 13.5 km ACT swath and a continuous ALT sampling. The city-mode differs from the nominal nadir pattern in the following ways: 1) the satellite makes a permanent pitch rotation to slow the projection of the line of sight on ground, leading to an ALT footprint size of 2.25 km (for the same 1.3s integration time); 2) the ACT footprint binning includes 15 pixels, leading to 6 ACT footprints with an ACT size of 2.25 km; and 3) the ACT swath is increased by making several ALT sweeps, each shifted by 13.5 km. For that purpose, the satellite makes additional pitch manoeuvres before and after flying over the target, to get a forward and backward viewing of the target, shifted by 13.5 km ACT using the pointing mirror to get contiguous spatial observations. Two configurations are implemented (Figure 2): 1) the two-sweep configuration has only forward and backward observations, leading to a ∼40 km ACT swath (2 x 13.5 km including the off-

https://doi.org/10.5194/egusphere-2022-749
Preprint. Discussion started: 8 September 2022

nadir pointing footprint deformation); and 2) the three-sweep configuration has forward, nadir, and backward observations, leading to a ∼60 km ACT swath. The allowed duration of each sweep mode leads to an ALT swath of ∼40 km.

2.2 Cloud screening

The MicroCarb science team will use ECMWF cloud forecasts to program city-mode measurements, in order to maximize the success of cloud-free observations. However, the cloud forecast has a limited precision and small-scale clouds still exist. Here, to realistically describe (and remove) scenes contaminated by clouds on the spatial scale of the observations, we use ERA5 total cloud cover reanalysis data at 0.25°×0.25° resolution (Hersbach et al., 2018) for the expected satellite equatorial overpass time (12:00 UTC) of MicroCarb. We use a downscaling method that assumes the dependence of the probability (f) of a cloud-free scene to its pixel size (s) and large-scale cloud cover (P) (Palmer et al., 2011):

$$f(P,s) = F_p(s)g(1-P), \tag{1}$$

where g defined as a constant factor for alignment between the instrument pixel and the cloud-free subgrid region, which we choose to be 1. The pixel size (s) of MicroCarb city-scan observing mode is approximately 2 km × 2 km. Using a constant alignment factor (g) will cause an overestimation of the probability for cloud-free observations at high cloud cover and an underestimation at low cloud cover. $F_p(s)$ is the penalty function accounting for the adverse effects on cloud-free probability when the effective instrument pixel size is larger than the nominal 1 km^2 (Boesch et al., 2011):

$$F_p(s) = \frac{26.098s^{-0.45} + 10.18}{26.098 + 10.18}. \tag{2}$$

For an individual sampling, we generate a pseudo-random number between 0 to 1 and compare it with its cloud-free probability (f) to determine its quality flag (QF). If the pseudo-random number is smaller than its estimated probability (f), we define it as a cloud-free observation (QF=0). Otherwise, the sampling is defined as a cloud-contaminated observation (QF=1).

We report our results over Paris and London for three arbitrary days (5th, 15th and 25th) from the months of April, July, and December 2018 (Figure A1). For some of these days (five for Paris and three for London), we find that the cloud cover is 100%. In these cases, we arbitrarily halve the cloud cover to 50% to generate cloud-free scenes (Table A1). Out of the total 228 (two-sweep mode) and 342 (three-sweep mode) individual scenes over Paris and London, our method assigns 72 (two-sweep mode) and 124 (three-sweep mode) samplings to be cloud-free in Paris and 69 (two-sweep mode) and 119 (three-sweep mode) cloud-free samplings in London at 12:00 UTC on 15 April 2018, respectively (Figure 2).

2.3 Anthropogenic CO_2 emissions

We use the Open-source Data Inventory for Anthropogenic CO_2 (ODIAC, 2019 version) for monthly-mean fossil fuel emissions of CO_2 in Paris and London at a spatial resolution of 1 km × 1 km (Oda and Maksyutov, 2011; Oda et al., 2018). The data product uses satellite observations of nighttime light and power plant profiles (including emissions intensity and geographical location) to distribute country-level CO_2 emission estimates from fossil fuel combustion. We use ODIAC to guide our broader study domains for Paris and London, ensuring we include anthropogenic source regions that lie outside the spatial extent of

https://doi.org/10.5194/egusphere-2022-749
Preprint. Discussion started: 8 September 2022

MicroCarb city-mode configurations (Figures 3a and 3b). For our calculations we exclude large point sources (such as power plants and some industrial emission points that typically lie outside the urban core), whose emissions are typically more than ten times larger than other diffused (area) emissions in the study domains and will likely have lower uncertainties than other urban sectors. In addition, errors in the locations of these point sources diminish the ability to infer sub-city scale emissions (Oda et al., 2017; Roten et al., 2022). Paris emissions of CO_2 (1.71 tCO_2 s^{-1} in April 2018) are concentrated in the city centre, home to about 2.17 million people (The National Institute of Statistics and Economic Studies). They are 1.4 times the size of those from London (1.25 tCO_2 s^{-1}), home to about 8.9 million people (United Nations - World Population Prospects), where emissions are aligned in the East-West direction along the Thames River.

2.4 Urban biosphere CO_2 fluxes

We use the SMUrF (Solar-Induced Fluorescence for Modeling Urban biogenic Fluxes) model (Wu et al., 2021) to estimate the net ecosystem exchange (NEE) across Paris and London. SMUrF estimates gross primary productivity (GPP) using OCO-2-derived solar-induced chlorophyll fluorescence (SIF) (Zhang et al., 2018) and neural networks to determine the relationship between ecosystem respiration and air and soil temperatures and GPP. SMUrF determines biome-specific model parameters by aggregating multiple flux tower sites from similar biomes across the globe to describe urban biogenic fluxes. We interpolate NEE values to the same grid used by ODIAC.

We evaluate SMUrF NEE estimates in France and UK by using eddy-covariance flux measurements from the European Fluxes Database Cluster: five sites in France (FR-Aur, FR-Hes, FR-Lam, FR-LGt, FR-Pue) and two sites in UK (UK-AMo and UK-EBu). Details of each site can be found at http://www.europe-fluxdata.eu/home/sites-list. These flux sites correspond to a variety of land types, including croplands (CRO), deciduous broadleaf forests (DBF), permanent wetlands (WET), evergreen broadleaf forests (EBF), and grasslands (GRA). We acknowledge these sites are not located in urban areas due to the lack of sufficient urban biosphere flux measurements (only one urban flux site in London and the data are not public), thus this evaluation provides us with limited confidence to understand the gradients in atmospheric CO_2 across these cities. All flux data in France are from 2018 (same year as our model meteorology). In the absence of UK flux data from 2018 we use data from 2015 (UK-AMo) and 2011 (UK-EBu). The seasonal-mean NEEs simulated by SMUrF in July 2018 agree reasonably with the eddy-covariance flux data (r=0.98 and slope=1.07 for the ensemble mean of all sites), although there are differences between site-specific model and observed photosynthetic uptake due to random errors, interpolation errors, and different spatial and temporal scales (Figure A2). Figures 3c and 3d show the spatial distribution of urban biosphere CO_2 fluxes on the 15 April 2018. We find substantial biospheric uptake over Paris and London during this month, comparable to the magnitude of fossil fuel emissions but with peak values located in contrasting regions. As we discuss below, these different emission distributions have implications for inferring fossil fuel combustion fluxes from atmospheric data.

2.5 Atmospheric transport model

We use the column version of the Stochastic Time-Inverted Lagrangian Transport model (X-STILT) (Wu et al., 2018a; Fasoli et al., 2018; Lin et al., 2003) to link surface CO_2 fluxes to variations of atmospheric CO_2 mole fractions at the locations of

https://doi.org/10.5194/egusphere-2022-749
Preprint. Discussion started: 8 September 2022

satellite soundings (Figures A3 and A4). X-STILT traces the movement of air parcels backwards in time. For the purposes of this study, we use a typical averaging kernel profile of OCO-2 that describes the vertical sensitivity of the column observations to changes in CO_2 in the column. We apply this averaging kernel and pressure weighting functions to the model fields to describe the footprints of satellite-based atmospheric CO_2 observations. The footprints describe the sensitivity of CO_2 columns at the receptors (locations where the satellite observes the atmosphere) to upwind surface fluxes.

To drive air parcels in X-STILT we use Global Forecast System meteorological data with a horizontal resolution of 0.25 degree (GFS0.25) (National Centers for Environmental Prediction, National Weather Service, NOAA, U.S. Department of Commerce, 2015). At the receptor, 3000 air parcels evenly distributed from the surface to 3 km height are released from the atmospheric column of each observed scene. We simulate footprints for the cloud-free scenes sampled by MicroCarb. The sum of the convolution of footprints and the ODIAC and SMUrf fluxes represents the urban CO_2 enhancements from upwind CO_2 fluxes, as sampled by air parcels arriving at the locations of each observed scene.

2.6 Maximum *A Posteriori* inverse method

We use the Maximum *A Posteriori* (MAP) inverse method (Enting, 2002; Tarantola, 2004; Feng et al., 2009) in which we solve for *a posteriori* CO_2 emissions by minimizing a cost function that describes the mismatch between the model-calculated enhancements and the measurements, accounting for *a priori* and measurement uncertainties. Minimizing the cost function results in the following expressions:

$$\hat{\mathbf{x}} = \mathbf{x}_0 + (\mathbf{HB})^{\mathrm{T}}(\mathbf{HBH}^{\mathrm{T}} + \mathbf{R})^{-1}(\mathbf{y} - \mathbf{Hx}_0), \tag{3}$$

$$\hat{\mathbf{S}} = \mathbf{B} - (\mathbf{HB})^{\mathrm{T}}(\mathbf{HBH}^{\mathrm{T}} + \mathbf{R})^{-1}(\mathbf{HB}), \tag{4}$$

where $\hat{\mathbf{x}}$ and $\hat{\mathbf{S}}$ denote the *a posteriori* state of grid-based CO_2 emission estimates across a city and the associated error covariance matrix, respectively. $\mathbf{x_0}$ and $\mathbf{B}$ denote the *a priori* emissions and the associated error covariance matrix. The measurement vector $\mathbf{y}$, includes the atmospheric CO_2 column enhancements, with the associated errors described by the observation error covariance matrix $\mathbf{R}$ (including measurement errors and atmospheric transport errors). $\mathbf{H}$ denotes the Jacobian matrix that describes the sensitivity of atmospheric CO_2 column enhancements to changes in CO_2 emissions.

To evaluate the theoretical performance of the MicroCarb city-mode data on improving *a priori* knowledge of urban CO_2 emissions over Paris and London, we use an error reduction metric (η) that takes into account differences between the *a priori* and *a posteriori* error covariance matrices (Palmer et al., 2000):

$$\eta = \left[1 - \left(\frac{\hat{\mathbf{S}}_{i,i}}{\mathbf{B}_{i,i}}\right)^{1/2}\right] \times 100\%, \tag{5}$$

where the subscripts denote the diagonal elements of the error covariance matrices. The larger value of η the more reduction in uncertainty of CO_2 emissions due to using the atmospheric CO_2 measurements.

https://doi.org/10.5194/egusphere-2022-749
Preprint. Discussion started: 8 September 2022

2.7 Closed-loop numerical experiments

Figure 1 describes the experimental approach we take to assess the theoretical ability of MicroCarb city-scan mode measurements to quantify urban emissions of CO_2 from Paris and London. Here, we discuss the individual steps involved, following Wu et al. (2018b). We use the ODIAC emissions and the SMUrF fluxes, described above, as the true state. The corresponding CO_2 column enhancements are generated from the true fluxes by the column-mean X-STILT transport model, as described above. We then add realistic observation noise to each cloud-free scene (determined by the cloud coverage) based on estimates from detailed simulations of the MicroCarb instrument. The random measurement errors range between 0.4–1.6 ppm with a mean value of 0.93 ppm for both the two-sweep and three-sweep configurations over Paris and mean values of 0.88 ppm (two-sweep) and 0.91 ppm (three-sweep) over London (Figure A5). We add a realistic additional 20% random error to the urban CO_2 column enhancement to account for atmospheric transport errors (Deng et al., 2017; Lauvaux et al., 2019) assuming the transport model is unbiased. A more formal estimation of atmospheric transport errors would suggest more confidence than we have in our estimate of the uncertainty in the X-STILT model. We will examine the impacts of different transport errors (described by the observation error covariance matrix) on the error reduction (η) of flux inversion. Based on these error estimates in the observation error covariance matrix ($\mathbf{R}$), we generate synthetic observed CO_2 enhancements, which are assumed to be unbiased.

Evaluating our ability to reduce *a priori* flux errors (including systematic and random errors) is the primary objective of this study. We respectively assume a mean systematic and random flux error of 2 μmol m^{-2} s^{-1} for fossil fuel emissions (Oda et al., 2019; Wu et al., 2018b). The mean random error of the biological fluxes is estimated as 25% based on the eddy-covariance flux measurements at the ecosystem sites described above. The total systematic and random flux errors are constrained by the Chi-square test that should be closer to one. We use an eigenvalue decomposition method to generate *a priori* flux noise from the flux error covariance matrix ($\mathbf{B}$). The flux errors are spatially correlated with an exponentially decaying function of the distance between emission grids and the spatial correlation length is estimated to be 10 km (Saide et al., 2011; Wu et al., 2011). We then sample the resulting *a priori* distribution of CO_2 column enhancements where there are cloud-free measurements and use the MAP inverse method to infer the *a posteriori* flux estimates and associated uncertainties over Paris and London. We can assess the ability of using the synthetic measurements to retrieve the "true" urban emissions from Paris and London at different times throughout the year.

3 Results

We report our results over Paris and London for three arbitrary days (5th, 15th and 25th) from the months of April, July, and December 2018. This allows us to investigate the impacts of different cloud cover and wind fields on the flux inversion of the proposed MicroCarb sampling strategies, and to understand how seasonal changes in the urban biosphere will influence our ability to determine urban anthropogenic emissions of CO_2. In total, we report the results of nine scenarios. In terms of structuring our results, we first use the results on 15th April 2018 to demonstrate the effectiveness of the inversion system, and then generalize these results for all nine scenarios.

https://doi.org/10.5194/egusphere-2022-749
Preprint. Discussion started: 8 September 2022

3.1 Flux estimates on 15th April 2018

Figure 4 shows the spatial distribution of the true and *a priori* fossil fuel CO_2 fluxes over Paris and London. Application of our random and systematic errors, as part of the closed-loop experimental configuration, introduces a significant difference between the truth and *a priori* emissions (Figures A6a and A7a). We use cloud-free satellite measurements to sample urban CO_2 enhancements that correspond to these emissions, as observed by MicroCarb using its proposed two-sweep and three-sweep city mode configurations (Figure 2). The number of cloud-free data over Paris at 12:00 (UTC) on 15th April 2018 using the two-sweep and three-sweep observing modes is 72 and 124, respectively. The corresponding number of cloud-free data over London is 69 and 119, respectively. The *a posteriori* CO_2 fluxes over Paris (Figures 4c and 4d) and London (Figures 4g and 4h) illustrate that cloud-free MicroCarb observations can broadly retrieve the spatial structure and magnitude of the true emissions. The *a posteriori* emission optimized by the two-sweep configuration can retrieve the true integrated emission for Paris within 18% from an *a priori* state of 52% larger than the truth. Similarly, this configuration results in an *a posteriori* emission estimate for London that is within 28% of the true value from an initial *a priori* difference of 74%. The three-sweep mode performs better to retrieve the total emissions of the truth within 7% (Paris) and 21% (London). For both cities, the *a posteriori* uncertainty is approximately half that of its *a priori* value. The three-sweep configuration outperforms the two-sweep configuration due to a higher number of cloud-free observations. For this day, the X-STILT footprints, describing the sensitivity of column-averaged CO_2 measurements to urban emissions, come from south of both Paris (Figure A3b) and London (Figure A4b). Consequently, sizeable flux correction and error reduction are shown in the south of Paris (Figure A6) and London (Figure A7). The error reduction is more significant for the three-sweep configuration due to more cloud-free scenes.

Figure 5 shows the urban CO_2 column enhancements that correspond to the true, *a priori*, and *a posteriori* emissions. The *a posteriori* CO_2 enhancements are closer to the "perfect" observations (OBS), which are generated from the true emissions, demonstrating the effectiveness of using the MicroCarb city-mode samplings to correct flux errors and improve the estimation of urban CO_2 enhancements. The prior and posterior column CO_2 enhancements for Paris and London on 15th April 2018 range 0–4 ppm with mean values of the "perfect" observations 1.28±0.71 ppm over Paris and 0.67±0.46 ppm over London for the two-sweep mode, consistent with previous studies on other cities (Kort et al., 2012; Hedelius et al., 2017, 2018; Kiel et al., 2021). Variation in enhancements reflects the spatial distribution of emissions across the cities and the footprints related to local meteorological conditions.

3.2 Sensitivity to cloud cover and measurement uncertainty

We estimate the sensitivity of flux error reduction to observation uncertainties (including atmospheric transport errors) and the data availability to a different number of cloud-free scenes within the three-sweep configuration (Figure 6). The peak spatially averaged error reduction is approximately 18% with the observation uncertainty of 0.5 ppm and the largest number of measurements. The lowest error reduction is for the minimal data availability with 80% cloud cover. Moreover, the scenario of all data (342 OBS) with 1.25 ppm observation uncertainty shows similar error reduction to the scenario of clear sky with

https://doi.org/10.5194/egusphere-2022-749
Preprint. Discussion started: 8 September 2022

1 ppm observation uncertainty for both Paris and London, indicating better measurement precision can partially compensate for fewer measurements. For both cities, the sensitivity of error reduction to changes in the observation uncertainty are similar for different cloud coverage, with increasing cloud coverage resulting in a near-uniform decrease in the flux error reduction.

3.3 Influence of biogenic CO_2 fluxes

Figure 7 shows how the introduction of biospheric CO_2 fluxes can influence the ability to infer anthropogenic CO_2 emissions. For this calculation we use the same true and *a priori* fields for the anthropogenic emissions of CO_2 over Paris on 15th April 2018 (Figures 4a and 4b). The effect of adding biospheric CO_2 fluxes is to reduce the urban CO_2 enhancements. These smaller column enhancements, within the context of the measurement uncertainties, limit our ability to reduce the random and systematic flux errors we impose as part of our closed-loop experiment, and consequently to quantify correctly anthropogenic CO_2 emissions. The total *a posteriori* anthropogenic emission estimate over Paris inferred using the three-sweep mode is 2.19 $tCO_2\ s^{-1}$ (Figure 7a), which is further from the true state than the emission estimate for the same scenario but in the absence of biospheric fluxes (Figure 4d). The *a posteriori* uncertainty increases by 51% from 0.45 to 0.68 $tCO_2\ s^{-1}$ relative to the scenario without biospheric fluxes. The *a posteriori* flux noise is larger (Figure 7b) with a degraded error reduction (Figure 7c) relative to the scenario without biospheric fluxes (Figures A6f and A6g). We find that biospheric uptake reduces the signal to noise ratio in satellite measurements (Figure 7d), which limits the ability to retrieve the true anthropogenic CO_2 emissions. We acknowledge that the degree of the influence from biosphere is subject to the uncertainty of *a priori* biogenic fluxes, the separation of anthropogenic signals from net CO_2 measurements, and the scale of inverted fluxes.

3.4 Ensemble analysis of Paris and London scenes

We generalize the results for nine individual scenarios over Paris and London, distributed evenly between April, July, and December 2018 (Figures 8 and 9). The nine scenes differ because of different biospheric fluxes and meteorological conditions, including cloud cover and prevailing wind that impact the data availability and footprints. In general, all configurations improve the *a priori* estimate, the extent of which is determined by the number of cloud-free scenes over each city, the sweep configuration used, and the introduction of seasonal biospheric CO_2 fluxes. This general discussion is consistent with our analysis from the 15th April 2018, described above. The three-sweep observing mode results in the most accurate reproduction of true urban emissions over Paris and London due to a higher number of cloud-free scenes (Figure 8). Ignoring the impact of biospheric CO_2 fluxes, the mean values of error reduction (including systematic and random error corrections) are 39% (two-sweep) and 46% (three-sweep) for Paris and those values are 44% (two-sweep) and 50% (three-sweep) for London (Figures 9a and 9c). In Paris, the scenario that results in the largest improvement to the *a priori* estimate is on 25th December 2018. This is due to a greater number of cloud-free scenes (Table A1) and weakly dispersed footprints from the south of Paris (Figure A3i) that is correlated with the distribution of the *a priori* flux noise (Figure A6a). A contrasting scenario, associated with weak improvement to the *a priori* estimate, is over Paris on 5th July 2018. This is mainly due to the footprint originating from the north of the city (Figure A3d) and therefore insensitive to the *a priori* flux noise. Generally, scenarios associated with the weakest improvements are associated with the lowest number of cloud-free scenes, e.g., 25th April 2018 over Paris (Table A1). We

https://doi.org/10.5194/egusphere-2022-749
Preprint. Discussion started: 8 September 2022

find similar results over London. Our analysis suggests that cloud cover and prevailing wind (speed and direction) are both determinants of city-scan observations being able to infer accurately urban anthropogenic emissions of CO_2.

Including the impact of seasonal biospheric CO_2 fluxes generally reduces the associated atmospheric CO_2 column enhancements and consequently limits the ability to infer fossil fuel CO_2 emissions (Figures 8b and 8d), particularly during April and July when the biosphere is more active and the flux error reductions are 20–40% over Paris and London (Figures 9b and 9d). We acknowledge our results are dependent on the uncertainties estimated for these biospheric fluxes. Decreasing the uncertainty of the *a priori* biospheric CO_2 fluxes will strengthen the relationship between the data and simulated urban CO_2 enhancements that consequently contributes to accurately quantifying anthropogenic CO_2 emissions.

4 Conclusions and Discussion

We evaluate the ability of MicroCarb city-scan observing modes to infer sub-city scale anthropogenic CO_2 emissions with sufficient measurement accuracy and density. Both the two-sweep and three-sweep observing modes are able to reduce *a priori* flux errors for 20–40% (including bias and random errors) over Paris and London, and retrieve the emission spatial structures of the truth. The three-sweep mode generally outperforms the two-sweep mode due to a wider scan area with a higher number of cloud-free observations. Cloud cover and prevailing wind are two determinants of city-scan observations for inferring accurately urban anthropogenic emissions of CO_2. The inversion system corrects more flux errors when there is less cloud cover and the footprints cover the area correlated to the distribution of *a priori* flux noise. The column-averaged urban CO_2 enhancements are 0–4 ppm for the cities we examined, which is about 1% of atmospheric background concentration. Quantifying sub-city scale emissions requires improving the accuracy and precision of satellite-based CO_2 measurements. Moreover, the presence of biospheric CO_2 fluxes diminishes the ability to estimate anthropogenic CO_2 emissions. Combining additional trace gases that are emitted with CO_2 during combustion (e.g., CO or NO_2) can help to infer urban CO_2 emissions (Konovalov et al., 2016; Reuter et al., 2019; Hakkarainen et al., 2021; Park et al., 2021; Wu et al., 2022a), especially during the growing season when the land biosphere absorbs atmospheric CO_2.

Estimating the regional/local atmospheric background CO_2 column concentration is important for quantifying the magnitude of urban enhancements due to net urban emissions, including anthropogenic and biospheric CO_2. There are a range of methods being employed to determine the background, such as calculating the mean value of column CO_2 surrounding the city area (Kort et al., 2012), estimating a dynamic background derived from a two-step linear regression method (Ye et al., 2020), or using the independent TCCON data of a remote site to derive background concentration (Kiel et al., 2021). In this study we have been able to sidestep this issue but only because it is a closed-loop simulation. For inversions with real MicroCarb data, we will need to consider an additional uncertainty associated with the calculation of the elevated CO_2 column. In addition, This study makes the simplifying assumption of unbiased and uncorrelated atmospheric transport errors, but transport errors are likely to be correlated at the sub-city scale. Our simplifying assumptions yield the maximum flux error reduction for the proposed MicroCarb samplings and represent a best-case scenario for the level of error reduction that could be achieved by the MicroCarb city-scan observing modes.

https://doi.org/10.5194/egusphere-2022-749
Preprint. Discussion started: 8 September 2022

Seasonal biospheric uptake of CO_2 within and around major cities will weaken observed CO_2 gradients across cities that would otherwise be determined by anthropogenic emissions. The use of ^{14}C isotope and CO has been demonstrated to separate fossil and biogenic fluxes inferred by ground-based atmospheric CO_2 measurements (Turnbull et al., 2015; Basu et al., 2020; Miller et al., 2020; Wu et al., 2022b). There are number of candidate approaches to alleviate this challenge for satellite-based CO_2 inversions but none have been proven extensively. A coupled assimilation of CO_2 with other trace gases that are co-emitted with anthropogenic CO_2 emissions such as CO or NO_2 provides constraints of the activity rates of individual anthropogenic sectors but still require sector-based knowledge of emission factors. Likewise, being able to reliably relate net biospheric fluxes to data products observed from satellites could also help to isolate fossil fuel emissions of CO_2 from natural fluxes over cities.

Code and data availability. The ODIAC emission inventory is available at http://dx.doi.org/10.17595/20170411.001 hosted by the Center for Global Environmental Research, National Institute for Environmental Studies (https://db.cger.nies.go.jp/dataset/ODIAC/). Biogenic CO_2 flux estimates from SMUrF are available at https://doi.org/10.3334/ORNLDAAC/1899. The X-STILT model is available at https://github.com/uataq/X-STILT. Codes of this study are available upon request.

Author contributions. KW and PIP designed the experiments; KW conducted the calculations using the X-STILT model and input data provided by DW, DJ, and TO; KW and PIP analysed the results and wrote the paper, with comments from all co-authors.

Competing interests. The authors declare no competing interests.

Acknowledgements. KW and PIP gratefully acknowledge funding from the UK Space Agency. PIP also acknowledges support from the UK National Centre for Earth Observation funded by the National Environment Research Council (NE/R016518/1).

https://doi.org/10.5194/egusphere-2022-749
Preprint. Discussion started: 8 September 2022

References

Basu, S., Lehman, S. J., Miller, J. B., Andrews, A. E., Sweeney, C., Gurney, K. R., Xu, X., Southon, J., and Tans, P. P.: Estimating US fossil fuel CO_2 emissions from measurements of ^{14}C in atmospheric CO_2, Proceedings of the National Academy of Sciences, 117, 13 300–13 307, 2020.

Bertaux, J.-L., Hauchecorne, A., Lefèvre, F., Bréon, F.-M., Blanot, L., Jouglet, D., Lafrique, P., and Akaev, P.: The use of the 1.27 μm O_2 absorption band for greenhouse gas monitoring from space and application to MicroCarb, Atmospheric Measurement Techniques, 13, 3329–3374, 2020.

Boesch, H., Baker, D., Connor, B., Crisp, D., and Miller, C.: Global characterization of CO_2 column retrievals from shortwave-infrared satellite observations of the Orbiting Carbon Observatory-2 mission, Remote Sensing, 3, 270–304, 2011.

Bréon, F., Broquet, G., Puygrenier, V., Chevallier, F., Xueref-Remy, I., Ramonet, M., Dieudonné, E., Lopez, M., Schmidt, M., Perrussel, O., et al.: An attempt at estimating Paris area CO_2 emissions from atmospheric concentration measurements, Atmospheric Chemistry and Physics, 15, 1707–1724, 2015.

Bulkeley, H.: Cities and Climate Change, London: Routledge, 2013.

Cai, Z., Liu, Y., and Yang, D.: Analysis of X_{CO_2} retrieval sensitivity using simulated Chinese Carbon Satellite (TanSat) measurements, Science China Earth Sciences, 57, 1919–1928, 2014.

Chaouad, R. and Verzeroli, M.: The urbanization of the world: Facts and challenges, Revue internationale et strategique, pp. 47–65, 2018.

Crisp, D., Pollock, H. R., Rosenberg, R., Chapsky, L., Lee, R. A., Oyafuso, F. A., Frankenberg, C., O'Dell, C. W., Bruegge, C. J., Doran, G. B., et al.: The on-orbit performance of the Orbiting Carbon Observatory-2 (OCO-2) instrument and its radiometrically calibrated products, Atmospheric Measurement Techniques, 10, 59–81, 2017.

Davis, K. J., Deng, A., Lauvaux, T., Miles, N. L., Richardson, S. J., Sarmiento, D. P., Gurney, K. R., Hardesty, R. M., Bonin, T. A., Brewer, W. A., et al.: The Indianapolis Flux Experiment (INFLUX): a test-bed for developing urban greenhouse gas emission measurements, Elem Sci Anth, 5, 2017.

Deng, A., Lauvaux, T., Davis, K. J., Gaudet, B. J., Miles, N., Richardson, S. J., Wu, K., Sarmiento, D. P., Hardesty, R. M., Bonin, T. A., et al.: Toward reduced transport errors in a high resolution urban CO_2 inversion system, Elem Sci Anth, 5, 2017.

Eldering, A., Wennberg, P., Crisp, D., Schimel, D., Gunson, M., Chatterjee, A., Liu, J., Schwandner, F., Sun, Y., O'dell, C., et al.: The Orbiting Carbon Observatory-2 early science investigations of regional carbon dioxide fluxes, Science, 358, eaam5745, 2017.

Eldering, A., Taylor, T. E., O'Dell, C. W., and Pavlick, R.: The OCO-3 mission: measurement objectives and expected performance based on 1 year of simulated data, Atmospheric Measurement Techniques, 12, 2341–2370, 2019.

Enting, I. G.: Inverse Problems in Atmospheric Constituent Transport, Cambridge University Press, Cambridge, UK, 2002.

Fasoli, B., Lin, J. C., Bowling, D. R., Mitchell, L., and Mendoza, D.: Simulating atmospheric tracer concentrations for spatially distributed receptors: updates to the Stochastic Time-Inverted Lagrangian Transport model's R interface (STILT-R version 2), Geoscientific Model Development, 11, 2813–2824, 2018.

Feng, L., Palmer, P., Bösch, H., and Dance, S.: Estimating surface CO_2 fluxes from space-borne CO_2 dry air mole fraction observations using an ensemble Kalman Filter, Atmospheric chemistry and physics, 9, 2619–2633, 2009.

Finch, D. P., Palmer, P. I., and Zhang, T.: Automated detection of atmospheric NO_2 plumes from satellite data: a tool to help infer anthropogenic combustion emissions, Atmospheric Measurement Techniques, 15, 721–733, 2022.

https://doi.org/10.5194/egusphere-2022-749
Preprint. Discussion started: 8 September 2022

Goldberg, D. L., Lu, Z., Oda, T., Lamsal, L. N., Liu, F., Griffin, D., McLinden, C. A., Krotkov, N. A., Duncan, B. N., and Streets, D. G.: Exploiting OMI NO_2 satellite observations to infer fossil-fuel CO_2 emissions from US megacities, Science of The Total Environment, 695, 133 805, 2019.

Hakkarainen, J., Ialongo, I., and Tamminen, J.: Direct space-based observations of anthropogenic CO_2 emission areas from OCO-2, Geophysical Research Letters, 43, 11–400, 2016.

Hakkarainen, J., Szeląg, M. E., Ialongo, I., Retscher, C., Oda, T., and Crisp, D.: Analyzing nitrogen oxides to carbon dioxide emission ratios from space: A case study of Matimba Power Station in South Africa, Atmospheric Environment: X, 10, 100 110, 2021.

Hedelius, J. K., Feng, S., Roehl, C. M., Wunch, D., Hillyard, P. W., Podolske, J. R., Iraci, L. T., Patarasuk, R., Rao, P., O'Keeffe, D., et al.: Emissions and topographic effects on column CO_2 (X_{CO_2}) variations, with a focus on the Southern California Megacity, Journal of Geophysical Research: Atmospheres, 122, 7200–7215, 2017.

Hedelius, J. K., Liu, J., Oda, T., Maksyutov, S., Roehl, C. M., Iraci, L. T., Podolske, J. R., Hillyard, P. W., Liang, J., Gurney, K. R., et al.: Southern California megacity CO_2, CH_4, and CO flux estimates using ground-and space-based remote sensing and a Lagrangian model, Atmospheric Chemistry and Physics, 18, 16 271–16 291, 2018.

Helfter, C., Tremper, A. H., Halios, C. H., Kotthaus, S., Bjorkegren, A., Grimmond, C. S. B., Barlow, J. F., and Nemitz, E.: Spatial and temporal variability of urban fluxes of methane, carbon monoxide and carbon dioxide above London, UK, Atmospheric Chemistry and Physics, 16, 10 543–10 557, 2016.

Hersbach, H., Bell, B., Berrisford, P., Biavati, G., Horányi, A., Muñoz Sabater, J., Nicolas, J., Peubey, C., Radu, R., Rozum, I., et al.: ERA5 hourly data on single levels from 1979 to present, Copernicus Climate Change Service (C3S) Climate Data Store (CDS), 10, 2018.

Ionov, D. V., Makarova, M. V., Hase, F., Foka, S. C., Kostsov, V. S., Alberti, C., Blumenstock, T., Warneke, T., and Virolainen, Y. A.: The CO_2 integral emission by the megacity of St Petersburg as quantified from ground-based FTIR measurements combined with dispersion modelling, Atmospheric Chemistry and Physics, 21, 10 939–10 963, 2021.

Janardanan, R., Maksyutov, S., Oda, T., Saito, M., Kaiser, J. W., Ganshin, A., Stohl, A., Matsunaga, T., Yoshida, Y., and Yokota, T.: Comparing GOSAT observations of localized CO_2 enhancements by large emitters with inventory-based estimates, Geophysical Research Letters, 43, 3486–3493, 2016.

Kiel, M., Eldering, A., Roten, D. D., Lin, J. C., Feng, S., Lei, R., Lauvaux, T., Oda, T., Roehl, C. M., Blavier, J.-F., et al.: Urban-focused satellite CO_2 observations from the Orbiting Carbon Observatory-3: A first look at the Los Angeles megacity, Remote Sensing of Environment, 258, 112 314, 2021.

Konovalov, I. B., Berezin, E. V., Ciais, P., Broquet, G., Zhuravlev, R. V., and Janssens-Maenhout, G.: Estimation of fossil-fuel CO_2 emissions using satellite measurements of "proxy" species, Atmospheric Chemistry and Physics, 16, 13 509–13 540, 2016.

Kort, E. A., Frankenberg, C., Miller, C. E., and Oda, T.: Space-based observations of megacity carbon dioxide, Geophysical Research Letters, 39, 2012.

Kunik, L., Mallia, D. V., Gurney, K. R., Mendoza, D. L., Oda, T., and Lin, J. C.: Bayesian inverse estimation of urban CO_2 emissions: results from a synthetic data simulation over Salt Lake City, UT, Elem Sci Anth, 7, 2019.

Lauvaux, T., Miles, N. L., Deng, A., Richardson, S. J., Cambaliza, M. O., Davis, K. J., Gaudet, B., Gurney, K. R., Huang, J., O'Keefe, D., et al.: High-resolution atmospheric inversion of urban CO_2 emissions during the dormant season of the Indianapolis Flux Experiment (INFLUX), Journal of Geophysical Research: Atmospheres, 121, 5213–5236, 2016.

Lauvaux, T., Díaz-Isaac, L. I., Bocquet, M., and Bousserez, N.: Diagnosing spatial error structures in CO_2 mole fractions and X_{CO_2} column mole fractions from atmospheric transport, Atmospheric Chemistry and Physics, 19, 12 007–12 024, 2019.

https://doi.org/10.5194/egusphere-2022-749
Preprint. Discussion started: 8 September 2022

Lei, R., Feng, S., Danjou, A., Broquet, G., Wu, D., Lin, J. C., O'Dell, C. W., and Lauvaux, T.: Fossil fuel CO_2 emissions over metropolitan areas from space: A multi-model analysis of OCO-2 data over Lahore, Pakistan, Remote Sensing of Environment, 264, 112 625, 2021.

Lin, J., Gerbig, C., Wofsy, S., Andrews, A., Daube, B., Davis, K., and Grainger, C.: A near-field tool for simulating the upstream influence of atmospheric observations: The Stochastic Time-Inverted Lagrangian Transport (STILT) model, Journal of Geophysical Research: Atmospheres, 108, 2003.

Liu, Y., Wang, J., Yao, L., Chen, X., Cai, Z., Yang, D., Yin, Z., Gu, S., Tian, L., Lu, N., et al.: The TanSat mission: preliminary global observations, Science Bulletin, 63, 1200–1207, 2018.

Lopez, M., Schmidt, M., Delmotte, M., Colomb, A., Gros, V., Janssen, C., Lehman, S., Mondelain, D., Perrussel, O., Ramonet, M., et al.: CO, NO_x and $^{13}CO_2$ as tracers for fossil fuel CO_2: results from a pilot study in Paris during winter 2010, Atmospheric Chemistry and Physics, 13, 7343–7358, 2013.

Makarova, M. V., Alberti, C., Ionov, D. V., Hase, F., Foka, S. C., Blumenstock, T., Warneke, T., Virolainen, Y. A., Kostsov, V. S., Frey, M., et al.: Emission Monitoring Mobile Experiment (EMME): an overview and first results of the St. Petersburg megacity campaign 2019, Atmospheric Measurement Techniques, 14, 1047–1073, 2021.

Mallia, D. V., Mitchell, L. E., Kunik, L., Fasoli, B., Bares, R., Gurney, K. R., Mendoza, D. L., and Lin, J. C.: Constraining urban CO_2 emissions using mobile observations from a light rail public transit platform, Environmental Science & Technology, 54, 15 613–15 621, 2020.

Masson-Delmotte, V., Zhai, P., Pörtner, H.-O., Roberts, D., Skea, J., Shukla, P. R., Pirani, A., Moufouma-Okia, W., Péan, C., Pidcock, R., et al.: Global warming of 1.5 °C, An IPCC Special Report on the impacts of global warming of 1.5 °C, 1, 2018.

Masson-Delmotte, V., Zhai, P., Pirani, A., Connors, S. L., Péan, C., Berger, S., Caud, N., Chen, Y., Goldfarb, L., Gomis, M., et al.: Climate change 2021: the physical science basis, Contribution of working group I to the sixth assessment report of the intergovernmental panel on climate change, p. 2, 2021.

Miller, J. B., Lehman, S. J., Verhulst, K. R., Miller, C. E., Duren, R. M., Yadav, V., Newman, S., and Sloop, C. D.: Large and seasonally varying biospheric CO_2 fluxes in the Los Angeles megacity revealed by atmospheric radiocarbon, Proceedings of the National Academy of Sciences, 117, 26 681–26 687, 2020.

Morino, I., Uchino, O., Inoue, M., Yoshida, Y., Yokota, T., Wennberg, P., Toon, G., Wunch, D., Roehl, C., Notholt, J., et al.: Preliminary validation of column-averaged volume mixing ratios of carbon dioxide and methane retrieved from GOSAT short-wavelength infrared spectra, Atmospheric Measurement Techniques, 4, 1061–1076, 2011.

National Centers for Environmental Prediction, National Weather Service, NOAA, U.S. Department of Commerce: NCEP GFS 0.25 Degree Global Forecast Grids Historical Archive, https://doi.org/10.5065/D65D8PWK, 2015.

Oda, T. and Maksyutov, S.: A very high-resolution (1 km $\times$ 1 km) global fossil fuel CO_2 emission inventory derived using a point source database and satellite observations of nighttime lights, Atmospheric Chemistry and Physics, 11, 543, 2011.

Oda, T., Lauvaux, T., Lu, D., Rao, P., Miles, N. L., Richardson, S. J., and Gurney, K. R.: On the impact of granularity of space-based urban CO_2 emissions in urban atmospheric inversions: A case study for Indianapolis, IN, Elementa: Science of the Anthropocene, 5, 2017.

Oda, T., Maksyutov, S., and Andres, R. J.: The Open-source Data Inventory for Anthropogenic CO_2, version 2016 (ODIAC2016): a global monthly fossil fuel CO_2 gridded emissions data product for tracer transport simulations and surface flux inversions, Earth System Science Data, 10, 87–107, 2018.

https://doi.org/10.5194/egusphere-2022-749
Preprint. Discussion started: 8 September 2022

Oda, T., Bun, R., Kinakh, V., Topylko, P., Halushchak, M., Marland, G., Lauvaux, T., Jonas, M., Maksyutov, S., Nahorski, Z., et al.: Errors and uncertainties in a gridded carbon dioxide emissions inventory, Mitigation and Adaptation Strategies for Global Change, 24, 1007–1050, 2019.

O'Dell, C. W., Eldering, A., Wennberg, P. O., Crisp, D., Gunson, M. R., Fisher, B., Frankenberg, C., Kiel, M., Lindqvist, H., Mandrake, L., et al.: Improved retrievals of carbon dioxide from Orbiting Carbon Observatory-2 with the version 8 ACOS algorithm, Atmospheric Measurement Techniques, 11, 6539–6576, 2018.

Palmer, P., Feng, L., and Bösch, H.: Spatial resolution of tropical terrestrial CO_2 fluxes inferred using space-borne column CO_2 sampled in different earth orbits: the role of spatial error correlations, Atmospheric Measurement Techniques, 4, 1995–2006, 2011.

Palmer, P. I., Barnett, J., Eyre, J., and Healy, S.: A nonlinear optimal estimation inverse method for radio occultation measurements of temperature, humidity, and surface pressure, Journal of Geophysical Research: Atmospheres, 105, 17 513–17 526, 2000.

Park, H., Jeong, S., Park, H., Labzovskii, L. D., and Bowman, K. W.: An assessment of emission characteristics of Northern Hemisphere cities using spaceborne observations of CO_2, CO, and NO_2, Remote Sensing of Environment, 254, 112 246, 2021.

Pascal, V., Buil, C., Loesel, J., Tauziede, L., Jouglet, D., and Buisson, F.: An improved microcarb dispersive instrumental concept for the measurement of greenhouse gases concentration in the atmosphere, in: International Conference on Space Optics—ICSO 2014, vol. 10563, pp. 1028–1036, SPIE, 2017.

Reuter, M., Buchwitz, M., Schneising, O., Krautwurst, S., O'Dell, C. W., Richter, A., Bovensmann, H., and Burrows, J. P.: Towards monitoring localized CO_2 emissions from space: co-located regional CO_2 and NO_2 enhancements observed by the OCO-2 and S5P satellites, Atmospheric Chemistry and Physics, 19, 9371–9383, 2019.

Roten, D., Lin, J. C., Kunik, L., Mallia, D., Wu, D., Oda, T., and Kort, E. A.: The Information Content of Dense Carbon Dioxide Measurements from Space: A High-Resolution Inversion Approach with Synthetic Data from the OCO-3 Instrument, Atmospheric Chemistry and Physics Discussions, pp. 1–43, 2022.

Saide, P., Bocquet, M., Osses, A., and Gallardo, L.: Constraining surface emissions of air pollutants using inverse modelling: method intercomparison and a new two-step two-scale regularization approach, Tellus B, 63, 360–370, 2011.

Sargent, M., Barrera, Y., Nehrkorn, T., Hutyra, L. R., Gately, C. K., Jones, T., McKain, K., Sweeney, C., Hegarty, J., Hardiman, B., et al.: Anthropogenic and biogenic CO_2 fluxes in the Boston urban region, Proceedings of the National Academy of Sciences, 115, 7491–7496, 2018.

Schwandner, F. M., Gunson, M. R., Miller, C. E., Carn, S. A., Eldering, A., Krings, T., Verhulst, K. R., Schimel, D. S., Nguyen, H. M., Crisp, D., et al.: Spaceborne detection of localized carbon dioxide sources, Science, 358, eaam5782, 2017.

Sierk, B., Fernandez, V., Bézy, J.-L., Meijer, Y., Durand, Y., Courrèges-Lacoste, G. B., Pachot, C., Löscher, A., Nett, H., Minoglou, K., et al.: The Copernicus CO_2M mission for monitoring anthropogenic carbon dioxide emissions from space, in: International Conference on Space Optics—ICSO 2020, vol. 11852, pp. 1563–1580, SPIE, 2021.

Suto, H., Kataoka, F., Kikuchi, N., Knuteson, R. O., Butz, A., Haun, M., Buijs, H., Shiomi, K., Imai, H., and Kuze, A.: Thermal and near-infrared sensor for carbon observation Fourier transform spectrometer-2 (TANSO-FTS-2) on the Greenhouse gases Observing SATellite-2 (GOSAT-2) during its first year in orbit, Atmospheric Measurement Techniques, 14, 2013–2039, 2021.

Tarantola, A.: Inverse Problem Theory and Methods for Model Parameter Estimation, SIAM, 2004.

Taylor, T. E., Eldering, A., Merrelli, A., Kiel, M., Somkuti, P., Cheng, C., Rosenberg, R., Fisher, B., Crisp, D., Basilio, R., et al.: OCO-3 early mission operations and initial (vEarly) X_{CO_2} and SIF retrievals, Remote Sensing of Environment, 251, 112 032, 2020.

https://doi.org/10.5194/egusphere-2022-749
Preprint. Discussion started: 8 September 2022

Turnbull, J., Sweeney, C., Karion, A., Newberger, T., Lehman, S. J., Tans, P. P., Davis, K. J., Lauvaux, T., Miles, N. L., Richardson, S. J., et al.: Toward quantification and source sector identification of fossil fuel CO_2 emissions from an urban area: results from the INFLUX experiment, Journal of Geophysical Research: Atmospheres, 120, 292–312, 2015.

Turner, A. J., Shusterman, A. A., McDonald, B. C., Teige, V., Harley, R. A., and Cohen, R. C.: Network design for quantifying urban CO_2 emissions: assessing trade-offs between precision and network density, Atmospheric Chemistry and Physics, 16, 13 465–13 475, 2016.

Verhulst, K. R., Karion, A., Kim, J., Salameh, P. K., Keeling, R. F., Newman, S., Miller, J., Sloop, C., Pongetti, T., Rao, P., et al.: Carbon dioxide and methane measurements from the Los Angeles Megacity Carbon Project–Part 1: calibration, urban enhancements, and uncertainty estimates, Atmospheric Chemistry and Physics, 17, 2017.

Wu, D., Lin, J. C., Fasoli, B., Oda, T., Ye, X., Lauvaux, T., Yang, E. G., and Kort, E. A.: A Lagrangian approach towards extracting signals of urban CO_2 emissions from satellite observations of atmospheric column CO_2 (XCO_2): X-Stochastic Time-Inverted Lagrangian Transport model ("X-STILT v1"), Geoscientific Model Development, 11, 4843–4871, 2018a.

Wu, D., Lin, J. C., Oda, T., and Kort, E. A.: Space-based quantification of per capita CO_2 emissions from cities, Environmental Research Letters, 15, 035 004, 2020.

Wu, D., Lin, J. C., Duarte, H. F., Yadav, V., Parazoo, N. C., Oda, T., and Kort, E. A.: A model for urban biogenic CO_2 fluxes: Solar-Induced Fluorescence for Modeling Urban biogenic Fluxes (SMUrF v1), Geoscientific Model Development, 14, 3633–3661, 2021.

Wu, D., Liu, J., Wennberg, P. O., Palmer, P. I., Nelson, R. R., Kiel, M., and Eldering, A.: Towards sector-based attribution using intra-city variations in satellite-based emission ratios between CO_2 and CO, Atmospheric Chemistry and Physics Discussions, pp. 1–32, 2022a.

Wu, K., Lauvaux, T., Davis, K. J., Deng, A., Coto, I. L., Gurney, K. R., and Patarasuk, R.: Joint inverse estimation of fossil fuel and biogenic CO_2 fluxes in an urban environment: An observing system simulation experiment to assess the impact of multiple uncertainties, Elem Sci Anth, 6, 2018b.

Wu, K., Davis, K. J., Miles, N. L., Richardson, S. J., Lauvaux, T., Sarmiento, D. P., Balashov, N. V., Keller, K., Turnbull, J., Gurney, K. R., et al.: Source decomposition of eddy-covariance CO_2 flux measurements for evaluating a high-resolution urban CO_2 emissions inventory, Environmental Research Letters, 17, 074 035, 2022b.

Wu, L., Bocquet, M., Lauvaux, T., Chevallier, F., Rayner, P., and Davis, K.: Optimal representation of source-sink fluxes for mesoscale carbon dioxide inversion with synthetic data, Journal of Geophysical Research: Atmospheres, 116, 2011.

Wunch, D., Toon, G. C., Blavier, J.-F. L., Washenfelder, R. A., Notholt, J., Connor, B. J., Griffith, D. W., Sherlock, V., and Wennberg, P. O.: The total carbon column observing network, Philosophical Transactions of the Royal Society A: Mathematical, Physical and Engineering Sciences, 369, 2087–2112, 2011.

Wunch, D., Wennberg, P. O., Osterman, G., Fisher, B., Naylor, B., Roehl, C. M., O'Dell, C., Mandrake, L., Viatte, C., Kiel, M., et al.: Comparisons of the orbiting carbon observatory-2 (OCO-2) X_{CO_2} measurements with TCCON, Atmospheric Measurement Techniques, 10, 2209–2238, 2017.

Yang, D., Liu, Y., Cai, Z., Chen, X., Yao, L., and Lu, D.: First global carbon dioxide maps produced from TanSat measurements, 2018.

Yang, E. G., Kort, E. A., Wu, D., Lin, J. C., Oda, T., Ye, X., and Lauvaux, T.: Using space-based observations and Lagrangian modeling to evaluate urban carbon dioxide emissions in the Middle East, Journal of Geophysical Research: Atmospheres, 125, e2019JD031 922, 2020.

Ye, X., Lauvaux, T., Kort, E. A., Oda, T., Feng, S., Lin, J. C., Yang, E. G., and Wu, D.: Constraining fossil fuel CO_2 emissions from urban area using OCO-2 observations of total column CO_2, Journal of Geophysical Research: Atmospheres, 125, e2019JD030 528, 2020.

Yokota, T., Yoshida, Y., Eguchi, N., Ota, Y., Tanaka, T., Watanabe, H., and Maksyutov, S.: Global concentrations of CO_2 and CH_4 retrieved from GOSAT: First preliminary results, Sola, 5, 160–163, 2009.

https://doi.org/10.5194/egusphere-2022-749
Preprint. Discussion started: 8 September 2022

515 Zhang, Y., Joiner, J., Alemohammad, S. H., Zhou, S., and Gentine, P.: A global spatially contiguous solar-induced fluorescence (CSIF) dataset using neural networks, Biogeosciences, 15, 5779–5800, 2018.

Zheng, B., Chevallier, F., Ciais, P., Broquet, G., Wang, Y., Lian, J., and Zhao, Y.: Observing carbon dioxide emissions over China's cities and industrial areas with the Orbiting Carbon Observatory-2, Atmospheric Chemistry and Physics, 20, 8501–8510, 2020.

https://doi.org/10.5194/egusphere-2022-749
Preprint. Discussion started: 8 September 2022

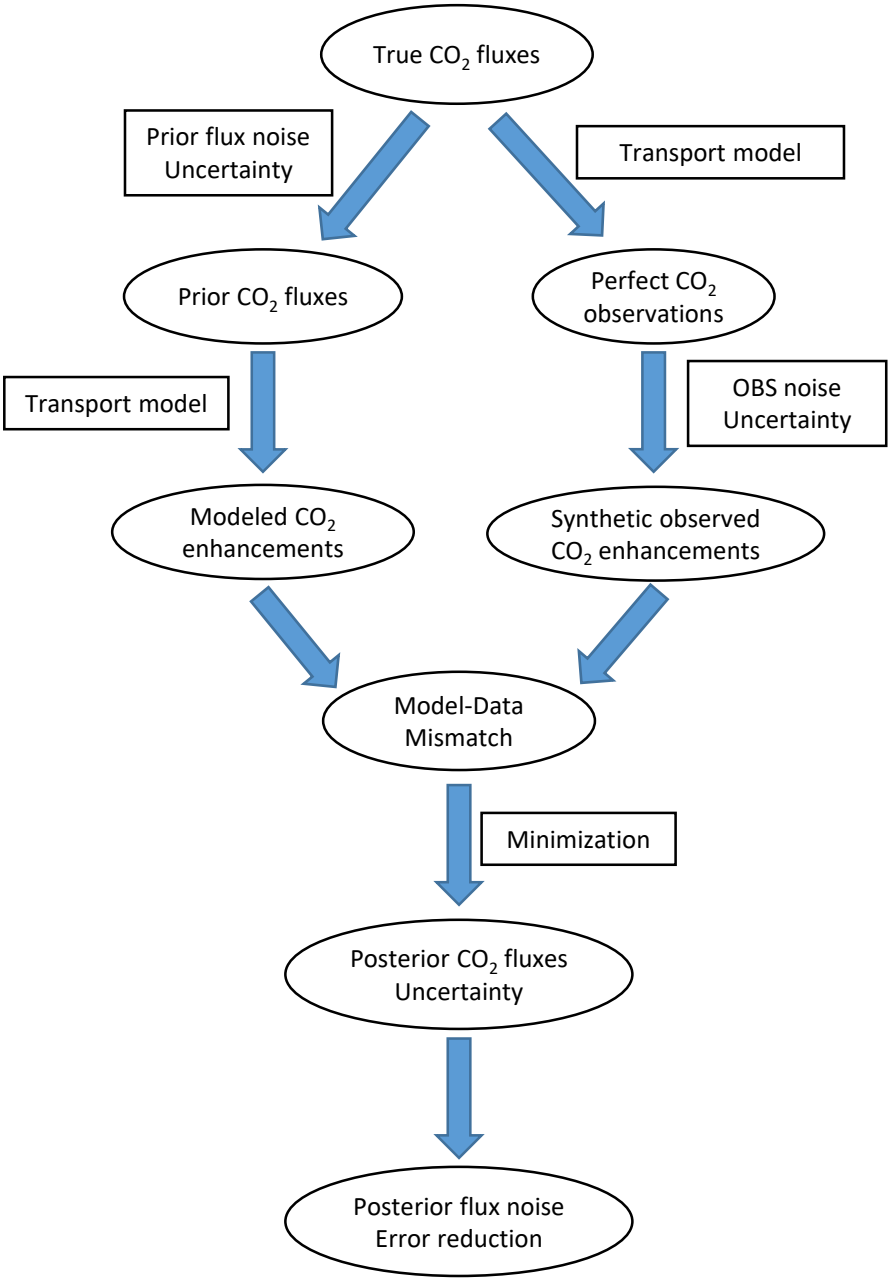

Figure 1. Flow chart of the Observing System Simulation Experiment (OSSE) for urban CO_2 inversion.

https://doi.org/10.5194/egusphere-2022-749
Preprint. Discussion started: 8 September 2022

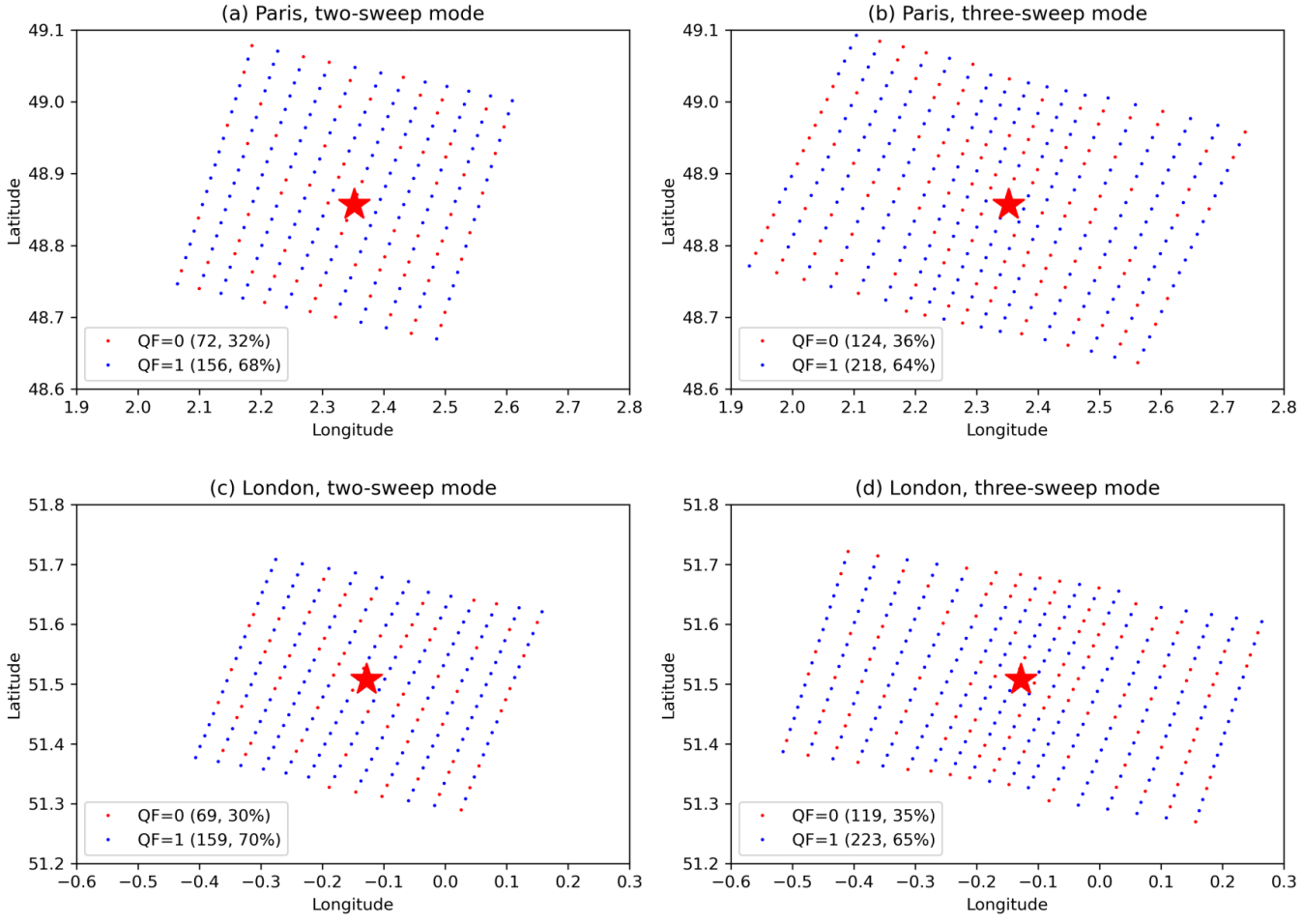

Figure 2. MicroCarb city-mode sampling patterns for the two-sweep and three-sweep modes in Paris (a and b) and London (c and d). Samplings are marked by quality flag (QF) using ERA5 total cloud cover at 12:00 UTC on 15 April 2018 (halve the cloud cover from one to 0.5). QF=0 means the samplings are cloud-free and QF=1 means the samplings are cloud-contaminated. Numbers in the parentheses are the number of observations and the percentage relative to the total number of observations for the two-sweep (228) and three-sweep (342) modes. The red star marks the city center.

https://doi.org/10.5194/egusphere-2022-749
Preprint. Discussion started: 8 September 2022

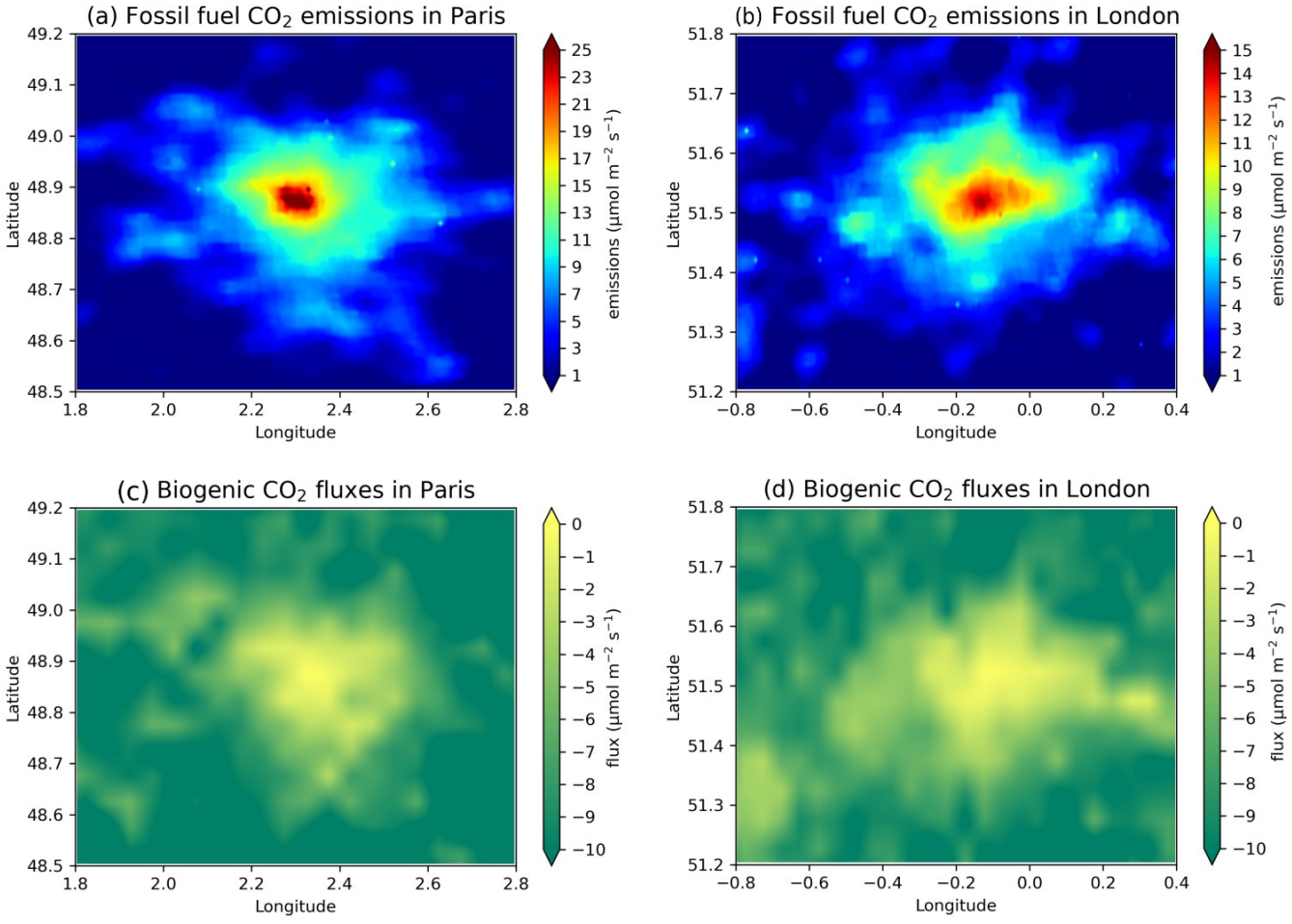

Figure 3. Monthly mean fossil fuel CO_2 emissions in April 2018 from ODIAC (without strong point sources) in Paris (a) and London (b). Biogenic CO_2 fluxes at 12:00 (UTC) on 15 April 2018 simulated by the SMUrF model in Paris (c) and London (d).

https://doi.org/10.5194/egusphere-2022-749
Preprint. Discussion started: 8 September 2022

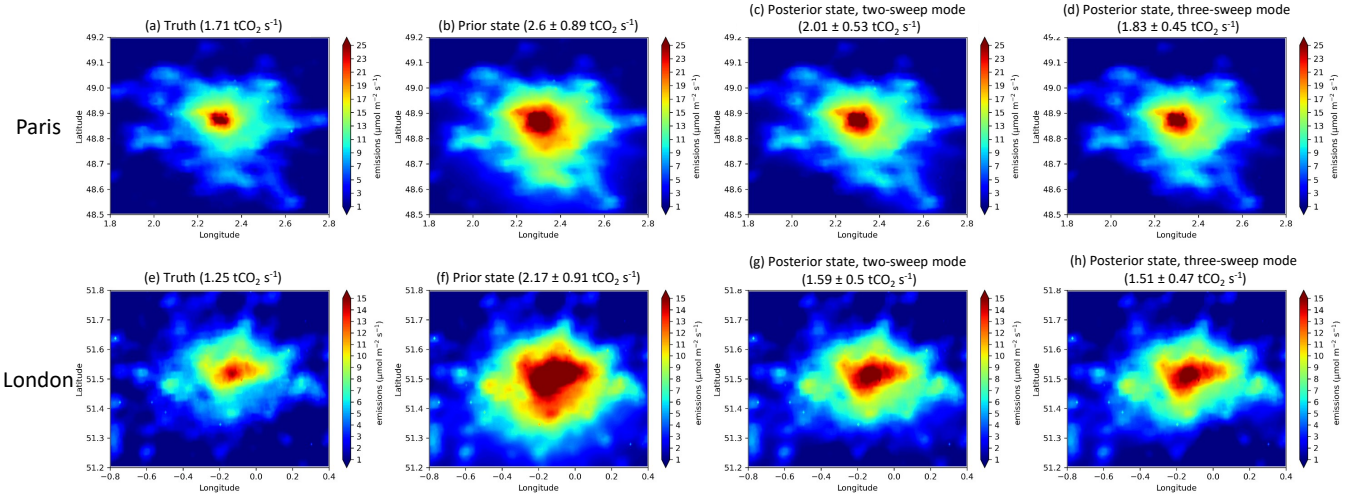

Figure 4. Truth, prior state, and posterior state based on the cloud-free samplings of the two-sweep and three-sweep modes in Paris (top panels, a to d) and London (bottom panels, e to h) at 12:00 (UTC) on 15 April 2018. The values in parentheses are the total CO_2 emissions within the domain (exclude strong point sources) and its uncertainty.

https://doi.org/10.5194/egusphere-2022-749
Preprint. Discussion started: 8 September 2022

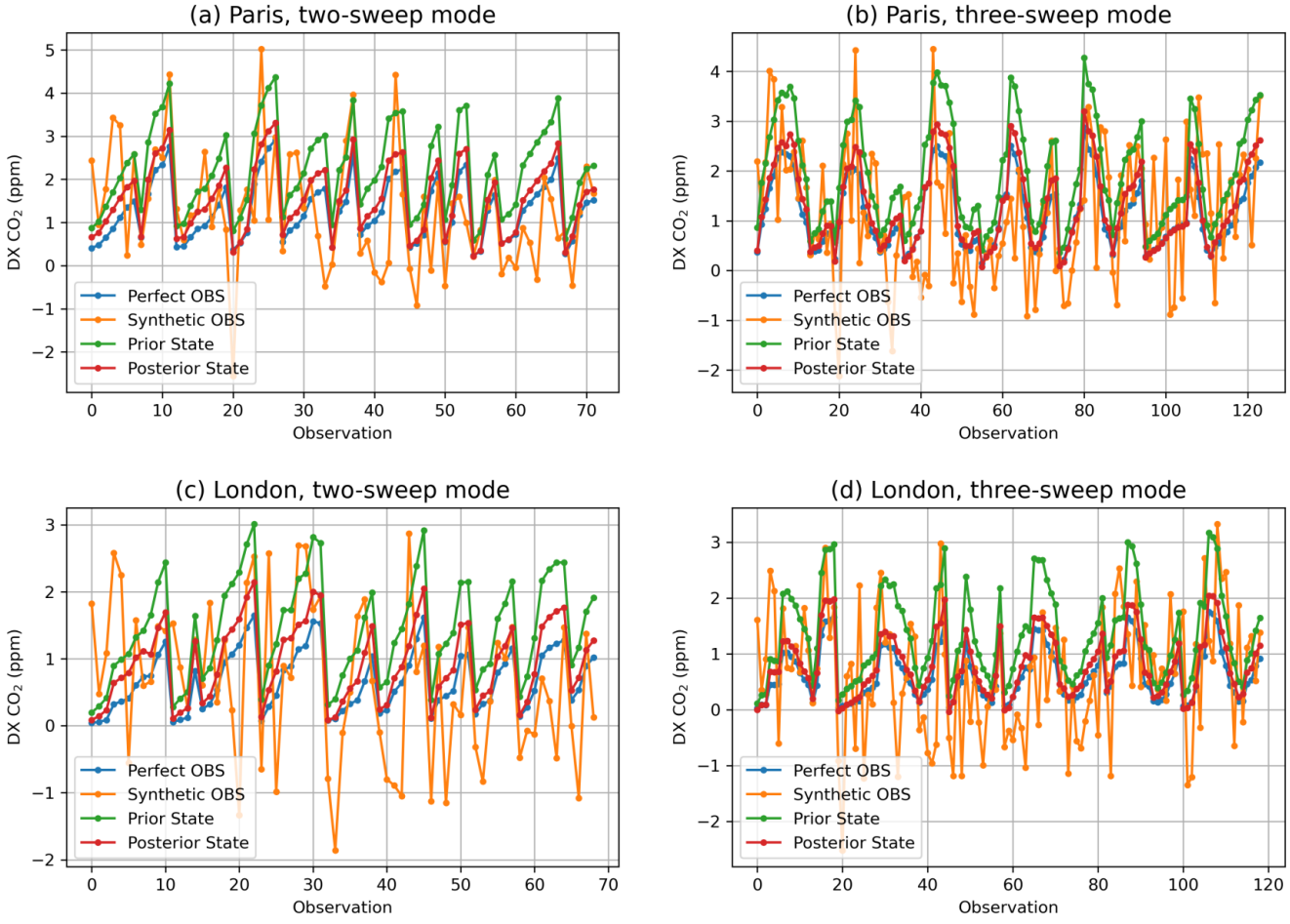

Figure 5. Urban CO_2 enhancements for the two-sweep and three-sweep modes in Paris (a and b) and London (c and d).

https://doi.org/10.5194/egusphere-2022-749
Preprint. Discussion started: 8 September 2022

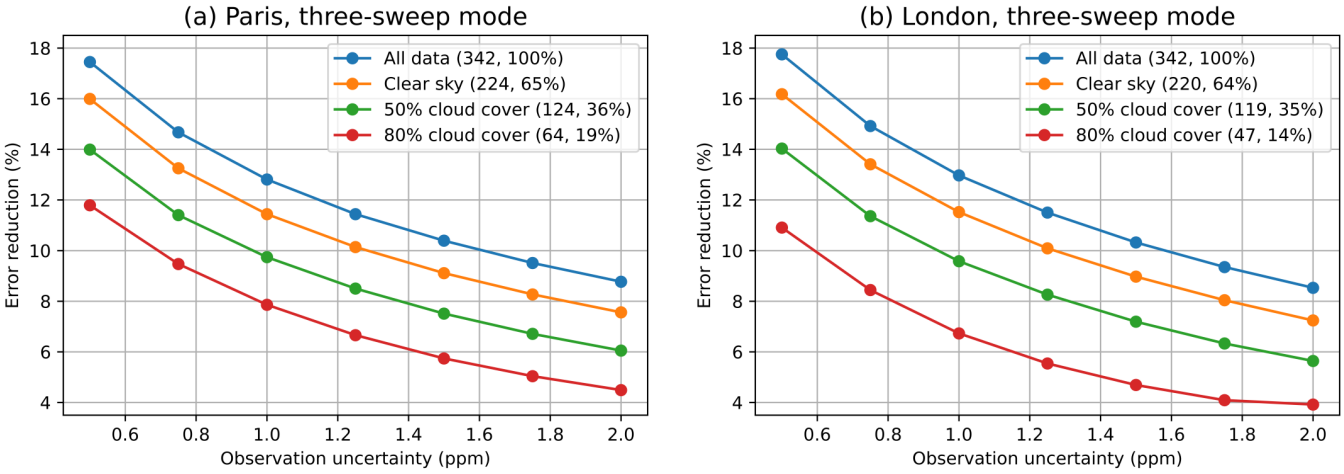

Figure 6. Spatially-averaged flux error reduction with the change of observation uncertainty under different sampling scenarios in Paris (a) and London (b). Numbers in the parentheses are the number of observations and the percentage relative to the total number of observations for the three-sweep mode (342).

https://doi.org/10.5194/egusphere-2022-749
Preprint. Discussion started: 8 September 2022

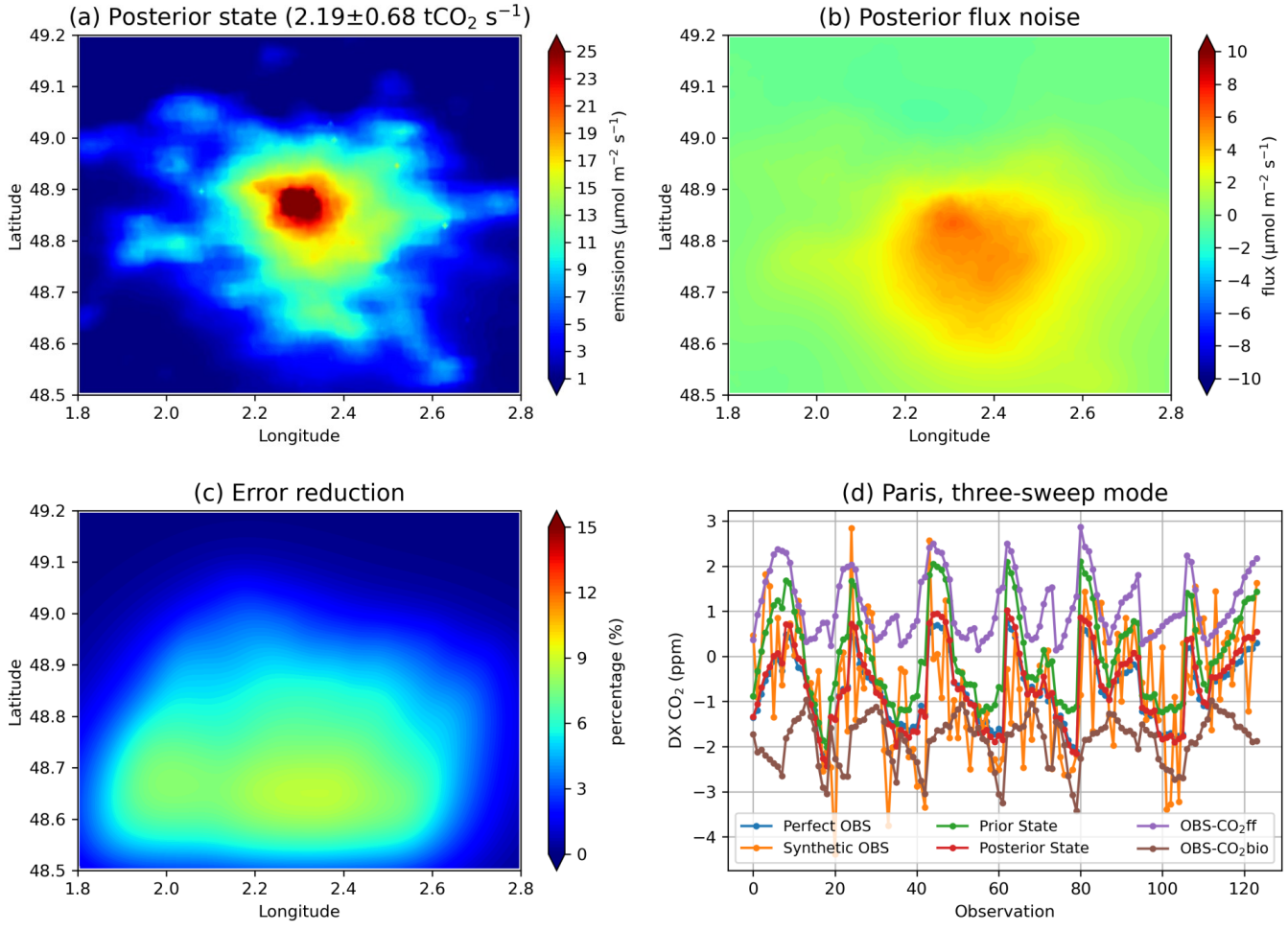

Figure 7. Posterior fossil fuel CO_2 fluxes (a), posterior flux noise (b), flux error reduction (c), and urban CO_2 enhancements (d) after including biogenic CO_2 fluxes in Paris for the three-sweep mode. The values in parentheses are the total emissions within the domain (exclude strong point sources) and its uncertainty.

https://doi.org/10.5194/egusphere-2022-749
Preprint. Discussion started: 8 September 2022

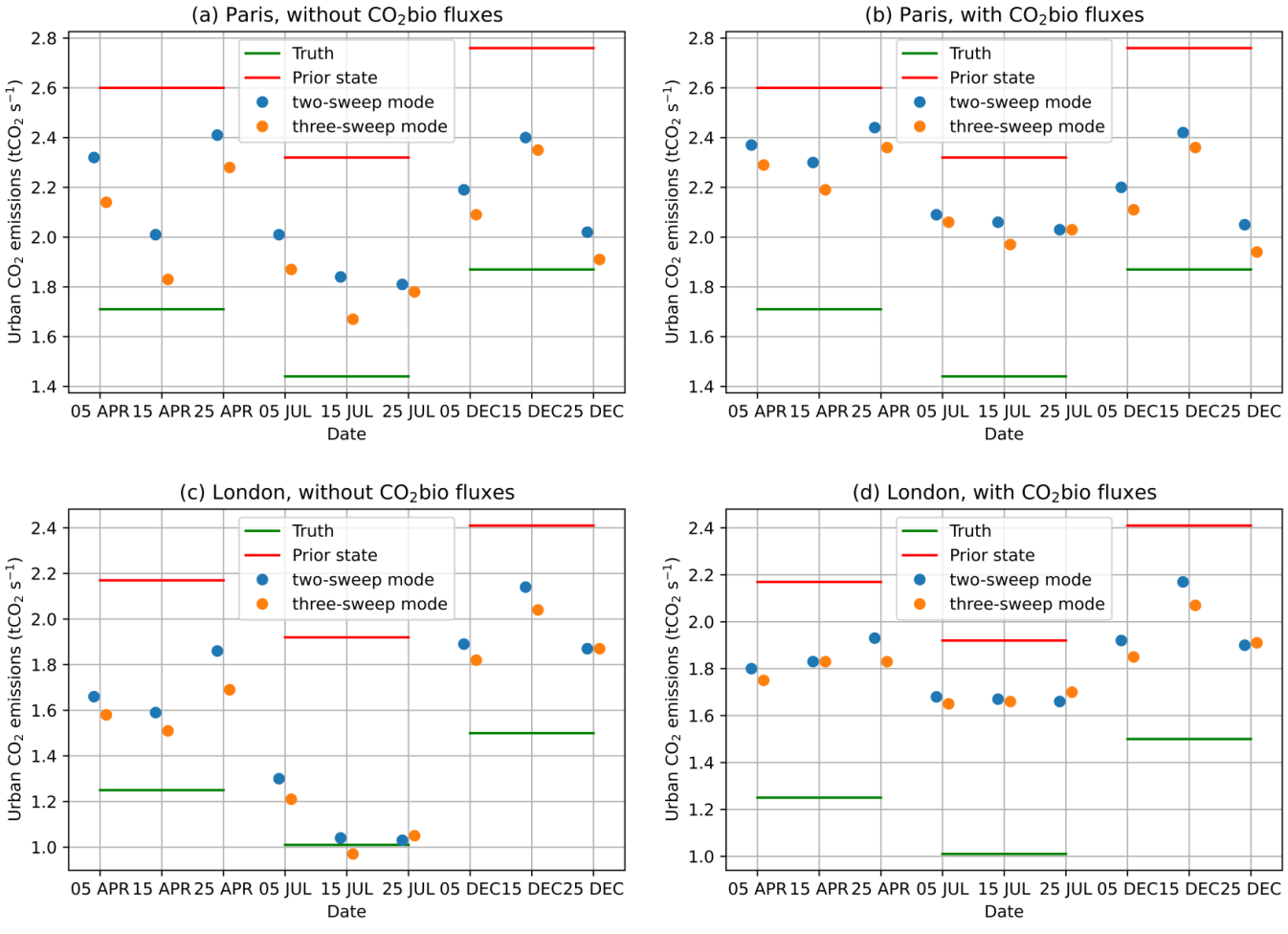

Figure 8. Total fossil fuel CO_2 emissions within the domain in Paris (a and b) and London (c and d) for different sampling scenarios. Left panels do not include the biogenic CO_2 flux component while right panels include the biogenic fluxes.

https://doi.org/10.5194/egusphere-2022-749
Preprint. Discussion started: 8 September 2022

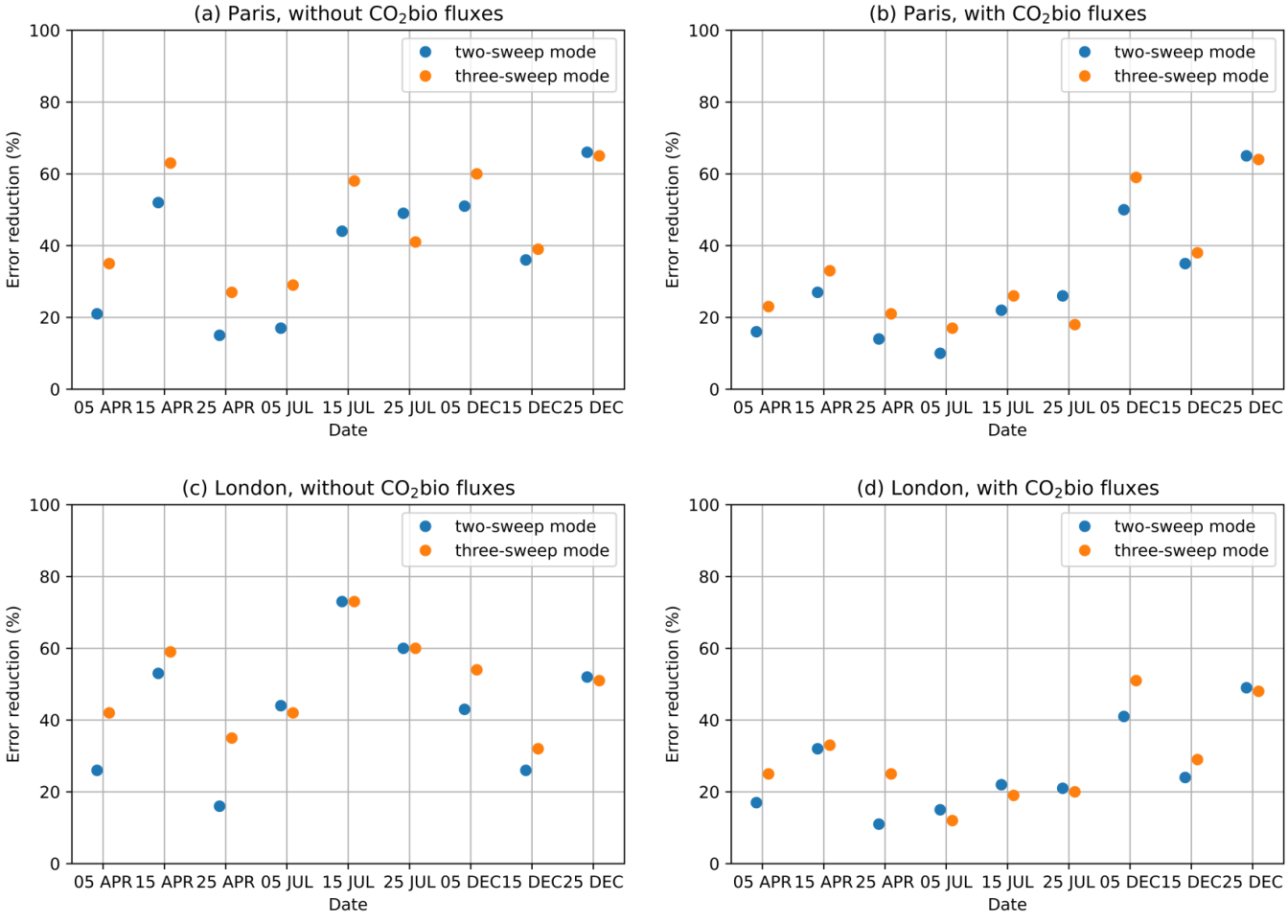

Figure 9. Similar as Figure 8, but for the error reduction of the total city-scale emissions.

https://doi.org/10.5194/egusphere-2022-749
Preprint. Discussion started: 8 September 2022

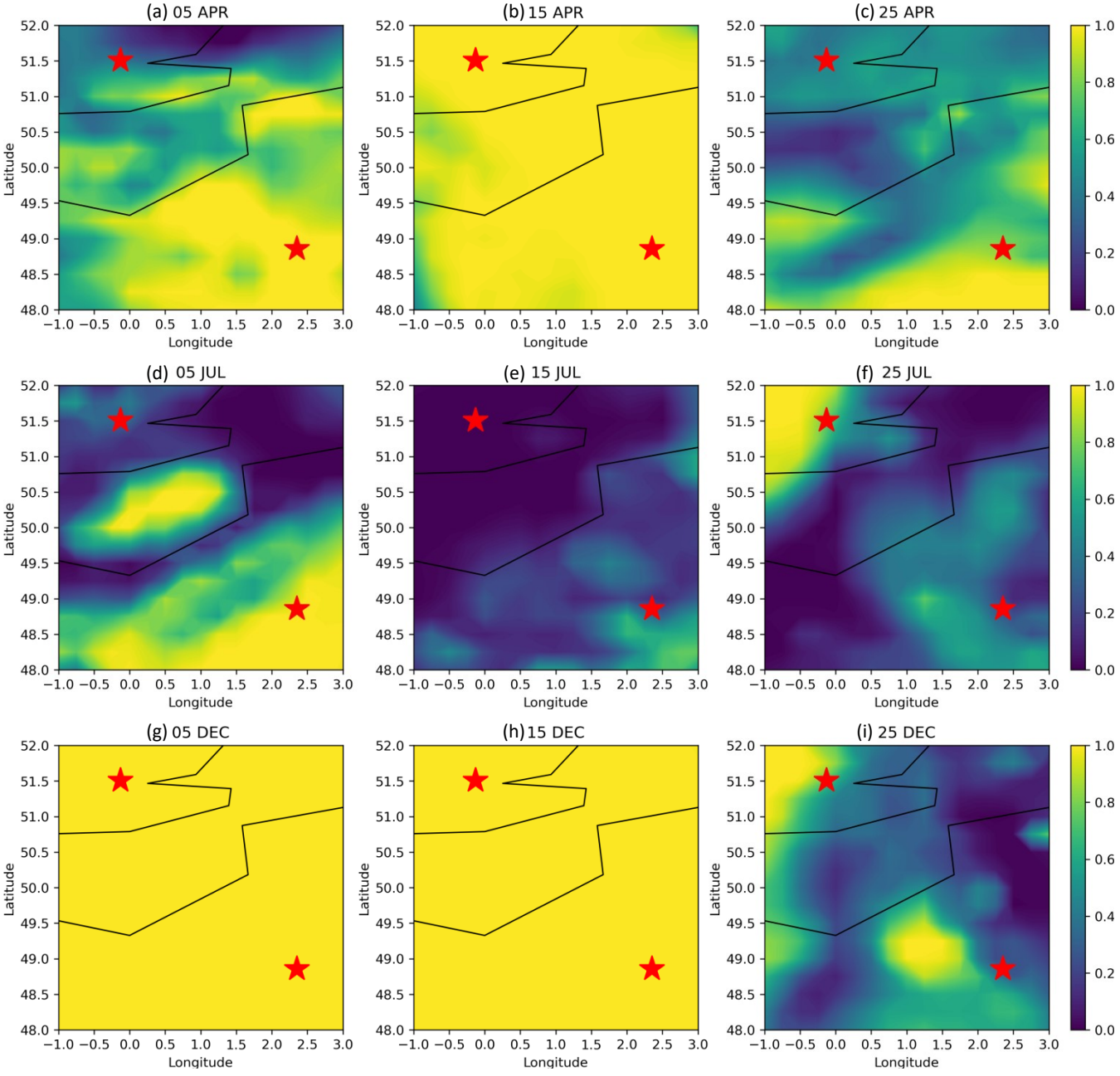

Figure A1. ERA5 total cloud cover at 12:00 (UTC) on the 5^{th}, 15^{th}, and 25^{th} in April, July, and December 2018 over Paris and London. The black line is the coastline and the red star marks the city center of Paris and London.

https://doi.org/10.5194/egusphere-2022-749
Preprint. Discussion started: 8 September 2022

Table A1. The number of cloud-free observations and its percentage relative to the total number of observations for the two-sweep (228) and three-sweep (342) modes in Paris and London. Bold numbers mark the dates that we artificially halve the cloud cover from one to 0.5, otherwise there are no cloud-free samplings at 12 UTC on those dates.

Two-sweep, Three-sweep		5	15	25
Paris	APR	**67 (29%), 114 (33%)**	**72 (32%), 124 (36%)**	27 (12%), 33 (10%)
	JUL	**89 (39%), 127 (37%)**	112 (49%), 185 (54%)	114 (50%), 169 (49%)
	DEC	**69 (30%), 128 (37%)**	**76 (33%), 108 (32%)**	101 (44%), 151 (44%)
London	APR	85 (37%), 151 (44%)	**69 (30%), 119 (35%)**	81 (36%), 130 (38%)
	JUL	121 (53%), 159 (46%)	148 (65%), 226 (66%)	48 (21%), 66 (19%)
	DEC	**78 (34%), 116 (34%)**	**70 (31%), 111 (32%)**	57 (25%), 59 (17%)

https://doi.org/10.5194/egusphere-2022-749
Preprint. Discussion started: 8 September 2022

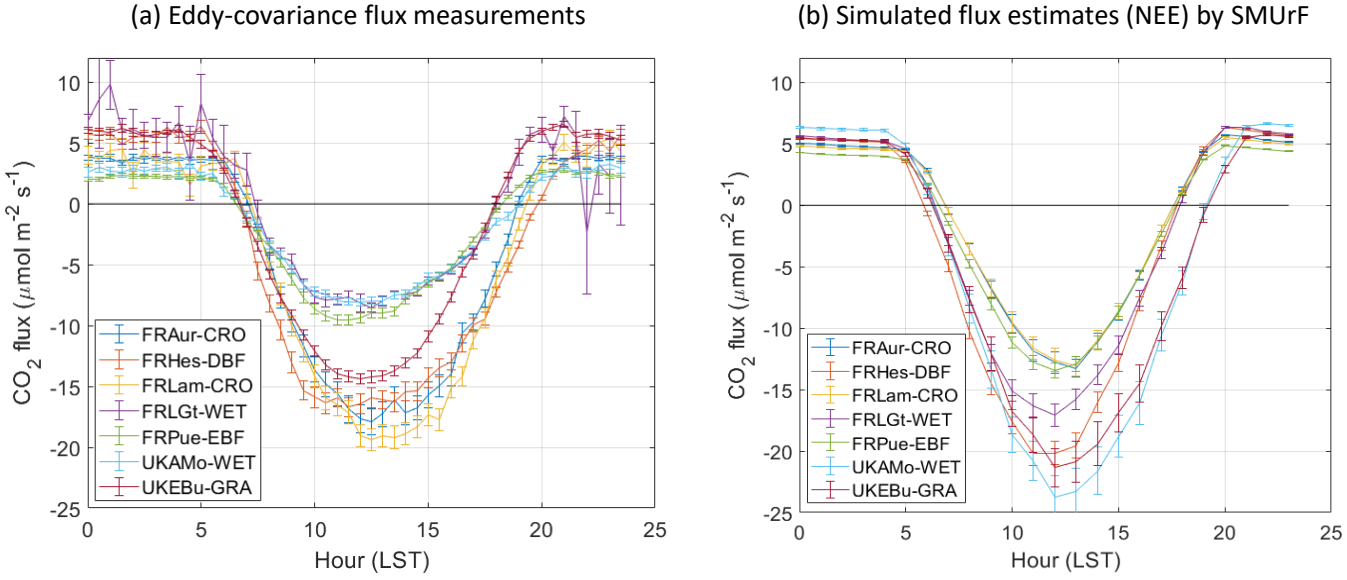

Figure A2. Diurnal variation of seasonally-averaged eddy-covariance flux measurements (a) and net ecosystem exchange (NEE) simulated by the SMUrF model (b). Error bars are the standard errors of the seasonal means. Flux data are downloaded from the European Fluxes Database Cluster, with five sites in France (FR-Aur, FR-Hes, FR-Lam, FR-LGt, FR-Pue) and two sites in UK (UK-AMo and UK-EBu). Site information is described on the website (http://www.europe-fluxdata.eu/home/sites-list). The land types are croplands (CRO), deciduous broadleaf forests (DBF), permanent wetlands (WET), evergreen broadleaf forests (EBF), and grasslands (GRA).

https://doi.org/10.5194/egusphere-2022-749
Preprint. Discussion started: 8 September 2022

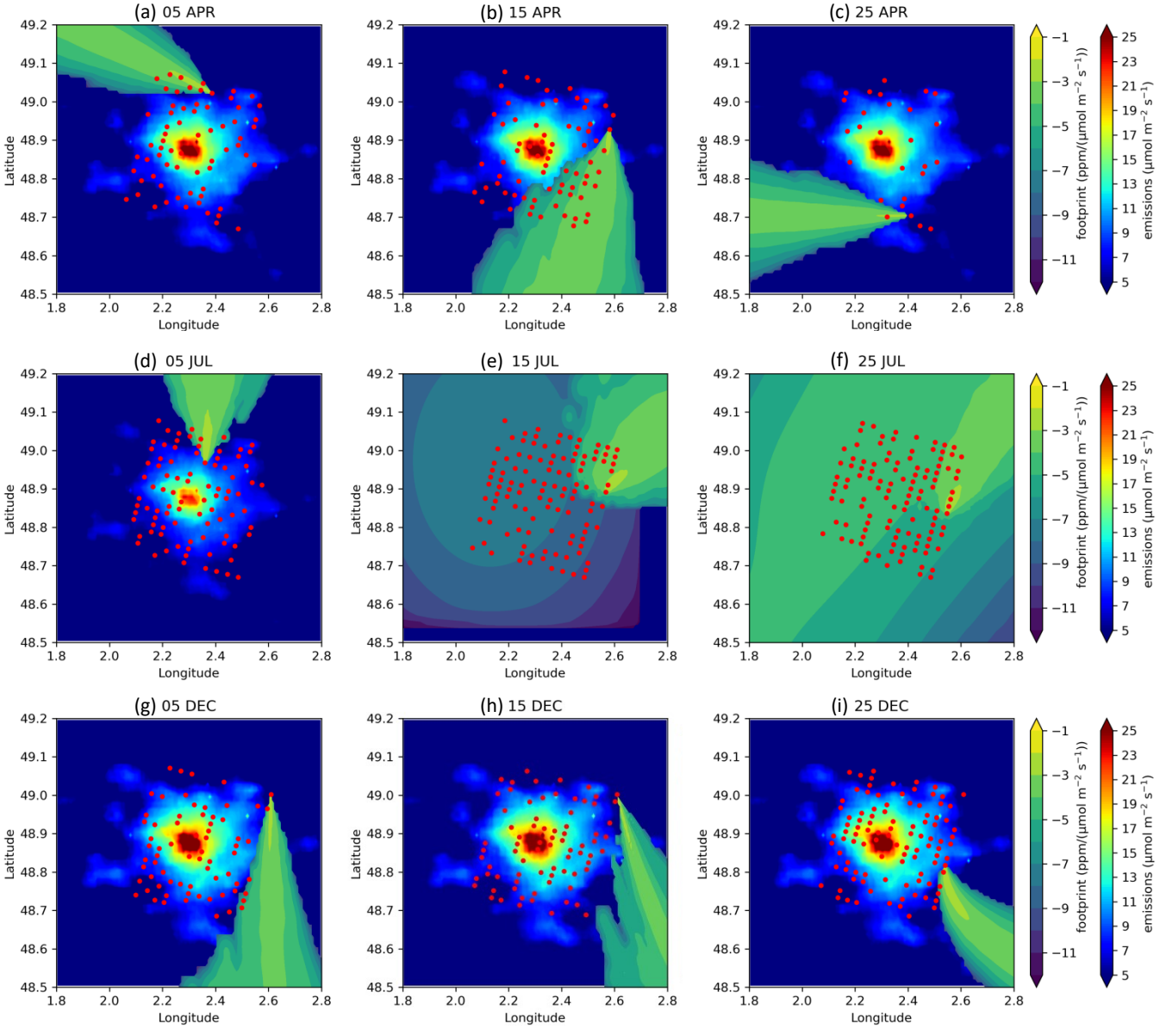

Figure A3. Monthly mean ODIAC emissions (without strong point sources) and the simulated footprint of a cloud-free sampling in the two-sweep mode at 12:00 (UTC) on the 5^{th}, 15^{th}, and 25^{th} in April, July, and December 2018 over Paris. The values of footprint are displayed on a logarithmic color scale.

https://doi.org/10.5194/egusphere-2022-749
Preprint. Discussion started: 8 September 2022

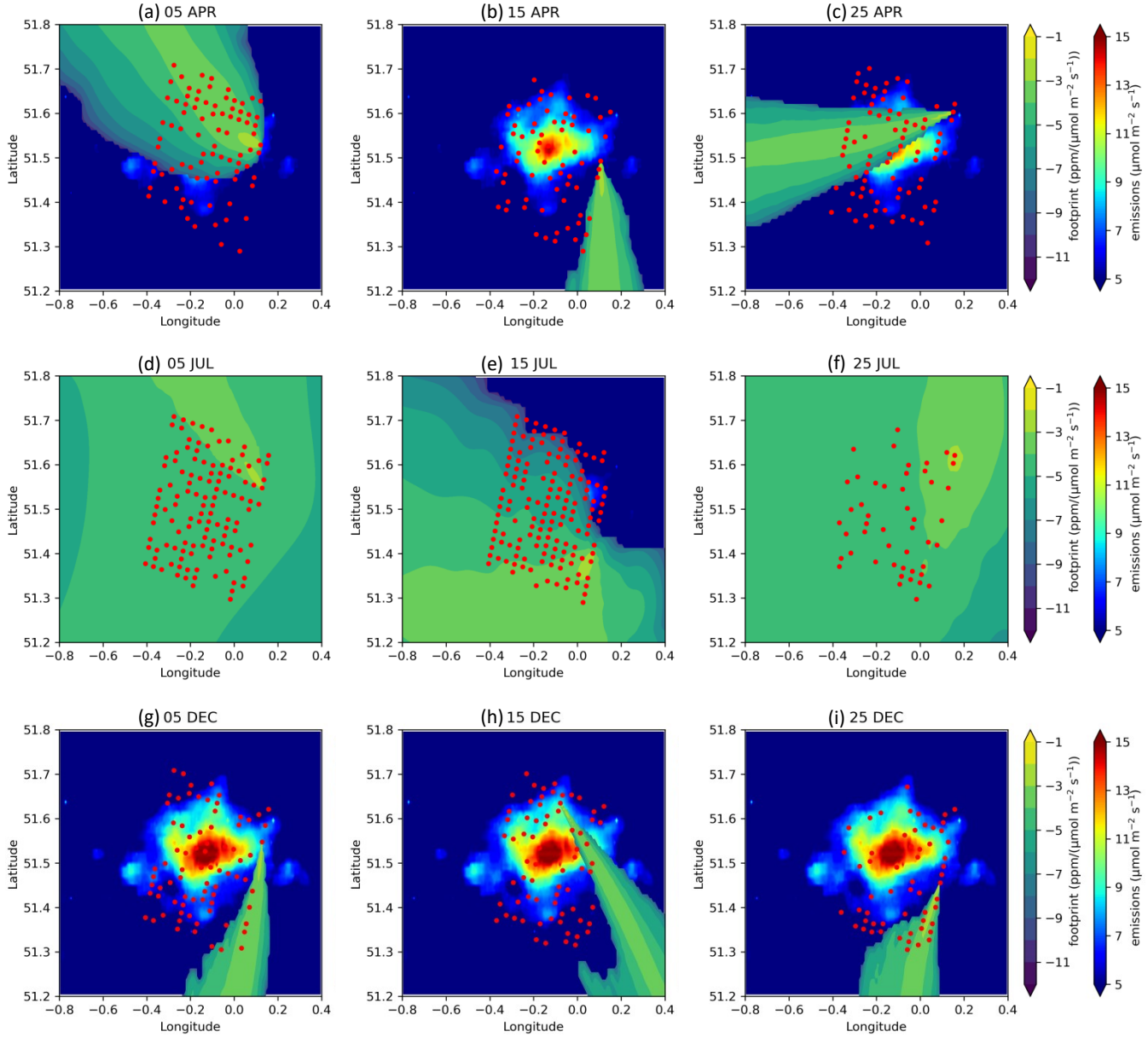

Figure A4. Same as Figure A3, but for London.

https://doi.org/10.5194/egusphere-2022-749
Preprint. Discussion started: 8 September 2022

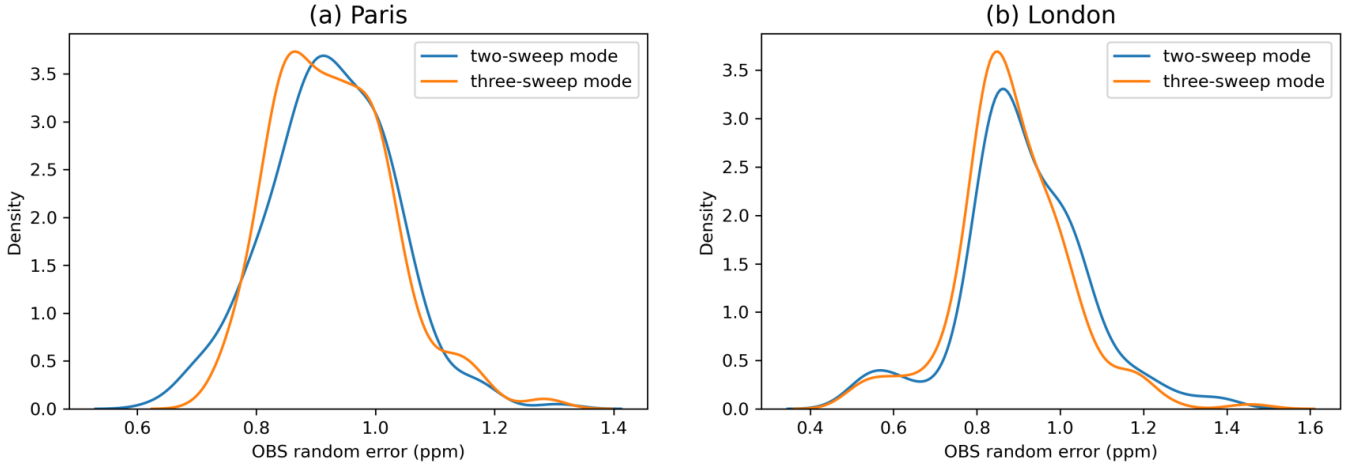

Figure A5. Probability density of the observation uncertainty (random measurement error) in Paris (a) and London (b).

https://doi.org/10.5194/egusphere-2022-749
Preprint. Discussion started: 8 September 2022

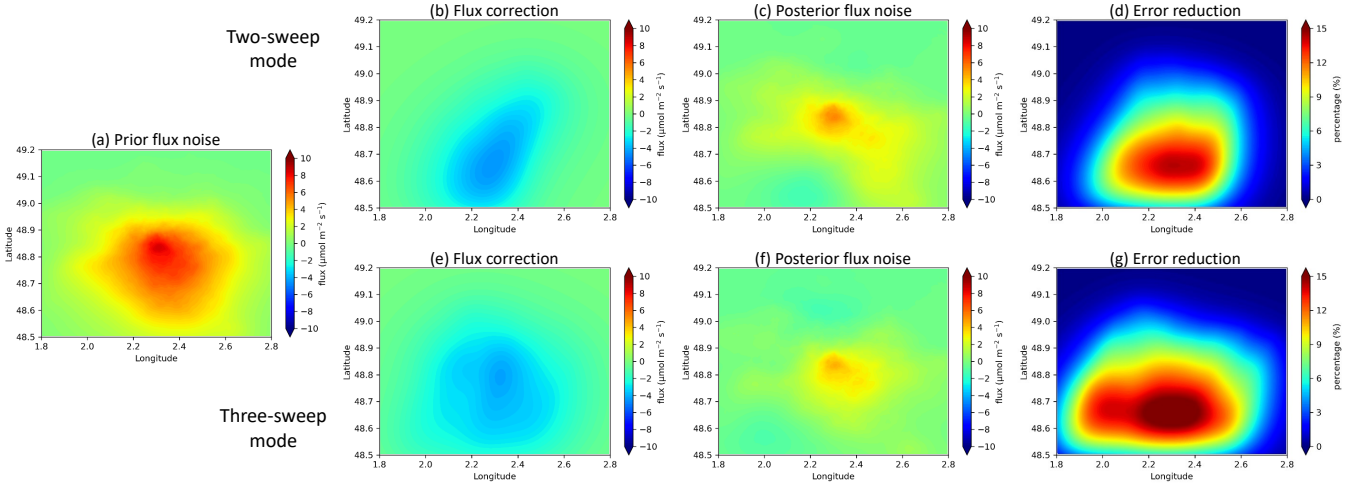

Figure A6. Prior flux noise (prior state minus truth), flux correction (posterior minus prior state), posterior flux noise (posterior state minus truth), and flux error reduction using the cloud-free samplings of the two-sweep (top panels, b to d) and three-sweep (bottom panels, e to g) modes in Paris.

https://doi.org/10.5194/egusphere-2022-749
Preprint. Discussion started: 8 September 2022

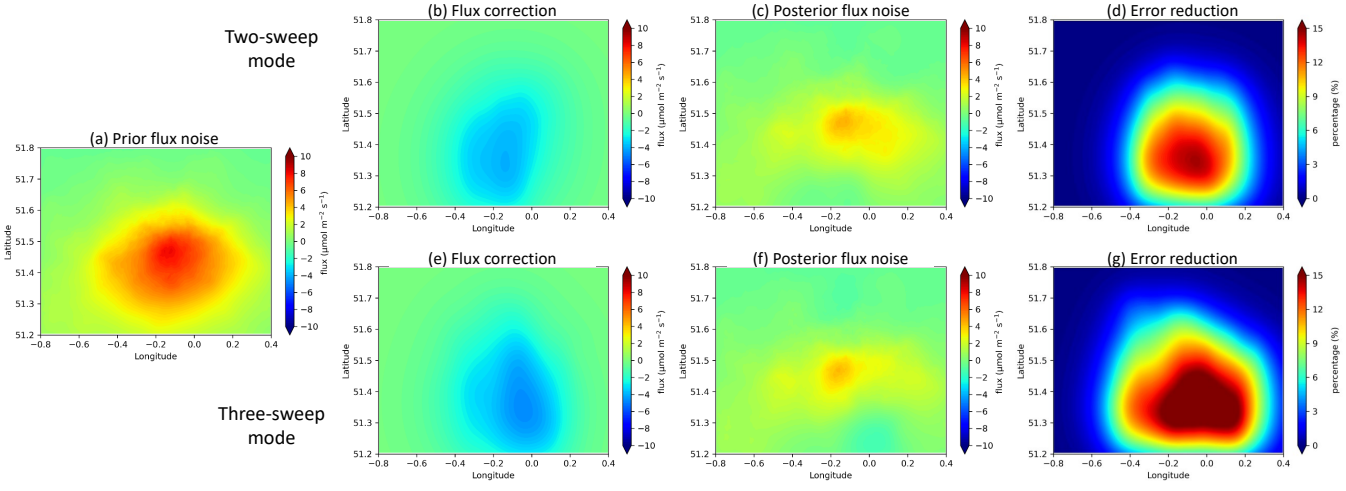

Figure A7. Same as Figure A6, but for London.